

**The effect of collimation on image quality and radiation safety in digital radiography of small animals**

by

Kevin James Koernig, DVM, MPH

A thesis submitted to the Graduate Faculty of  
Auburn University  
in partial fulfillment of the  
requirements for the Degree of  
Master of Science

Auburn, Alabama  
August 3, 2013

Copyright 2013 by Kevin James Koernig

Approved by

Judith A. Hudson, Chair, Professor, Department of Clinical Sciences  
William R. Brawner, Jr., Professor, Department of Clinical Sciences  
Gregory T. Almond, Assistant Clinical Professor, Department of Clinical Sciences

## Abstract

Collimating the primary x-ray beam to the specific area of anatomic interest has traditionally been strongly recommended to produce high quality radiographic images, even though some small animal patients can fit their entire torso on a single radiographic cassette or detector. However, modern digital radiography may allow for whole-body projections for these patients at similar quality to specific collimated projections. Lateral and ventrodorsal projections of 31 small dogs were obtained to evaluate the effect of collimation on the quality of the resulting digital radiograph. Each projection was performed using both a collimated and whole-body technique. Scatter radiation was detected during each exposure as well to determine the effect of collimation on radiation safety for veterinary personnel. The resulting images were cropped to portray only the thorax, and were evaluated by five radiologists blinded to the procedure used for each image. Visual grading characteristics analysis was performed. An overall trend towards higher image quality was found in the collimated approach compared to the whole-body, but in most cases this change was not significant. Overall image quality for the ventrodorsal images was found to be significantly better in the collimated approach compared to the whole-body. Evaluation of image histograms suggests that the application of digital processing and the look-up table differs between them, and this may account for a large portion of any quality difference. Over twice as much scatter radiation was detected during the whole-body images as during the collimated images. Overall image quality was rated as adequate to high for almost all images with both approaches. Adequate collimation remains recommended to provide the highest quality images with the lowest exposure to veterinary personnel.

## Table of Contents

Abstract.....	ii
Acknowledgments .....	v
List of Abbreviations .....	vi
List of Illustrations.....	vii
List of Tables .....	viii
I. Introduction .....	1
II. Literature Review .....	9
Digital Radiography .....	9
Radiation Safety and Scatter Radiation .....	18
Subhead .....	5
III. Materials and Methods .....	20
IV. Results .....	27
Image Quality .....	27
Scatter Radiation .....	50

VI. Discussion .....	51
V. References .....	58
Appendix A .....	64

## Acknowledgments

I would like to thank the faculty of the radiology section for making this project possible: Dr. Judith Hudson for all of her advice and guidance on this project, Dr. William Brawner and Dr. Gregory Almond for providing further advice and support as part of the committee, and Dr. John Hathcock and Dr. Robert Cole for taking part in the evaluation of images for the study. I am very grateful to Mike Anderson and Sevgi Kucuktas for advice and equipment essential to the radiation safety portion of this study. Also, I am very thankful for the students, faculty, and staff of the Auburn University College of Veterinary Medicine for volunteering the dogs needed for this study, and to the dogs themselves for being willing to tolerate the many strange things we humans ask them to do.

Finally, I am most of all grateful for my parents for making all that I have accomplished in life possible.

## List of Abbreviations

AUC	Area Under the Curve
CT	Computed Tomography
IC	Image Criteria
ROC	Receiver Operator Characteristic
VD	Ventrodorsal
VGA	Visual Grading Analysis
VGC	Visual Grading Characteristics
WB	Whole-Body

## List of Illustrations

Figure 1. Initial uncropped collimated lateral, whole-body lateral, collimated ventrodorsal, and whole-body ventrodorsal projections for one of the subjects .....	22
Figure 2. Final images from the same case as in figure 1 after digital cropping.....	23
Figure 3. VGC curve comparing overall ratings for images obtained with collimated approach compared to the whole-body approach. ....	41
Figure 4. Forest plots of AUCVGC and 95% confidence interval for all observers for the lateral images. ....	42
Figure 5. Forest plots of AUCVGC and 95% confidence interval for all observers for the ventrodorsal images. ....	43

## List of Tables

Table 1. European quality criteria for posterior-anterior (PA) chest radiographs in humans .....	15
Table 2. European quality criteria for lateral chest radiographs in humans .....	15
Table 3. Grades for the overall image quality and for the individual anatomic structures .....	24
Table 4. Individual anatomic structures evaluated on the lateral and ventrodorsal projections and the criteria for evaluation .....	25
Table 5. Spearman rank correlations of the grades for each observer pair for each criteria for the collimated and whole-body lateral images.....	29-30
Table 6. Spearman rank correlations of the grades for each observer pair for each criteria for the collimated and whole-body ventrodorsal images .....	31-32
Table 7. Counts (and frequencies) for each grade for each observer for the lateral images .....	34
Table 8. Counts (and frequencies) for each grade for each observer for the ventrodorsal images .....	35
Table 9. p values calculated from Wilcoxon signed-rank comparison of the grades for the collimated and whole body approach for each observer .....	37
Table 10. Mean grade for each observer for each criteria for each image type. ....	37
Table 11. Histograms of overall image quality grades for each observer for the lateral images .....	38
Table 12. Histograms of overall image quality grades for each observer for the lateral images .....	39
Table 13. The $AUC_{VGC}$ (and 95% confidence interval) for each observer for each criteria .....	41
Table 14. Grayscale histograms for all of the cropped images .....	45-49



## I. Introduction

Whole-body radiographic projections—projections in which the primary beam contains both the thoracic and abdominal cavities, rather than being collimated to a specific anatomic region—are a controversial subject in veterinary diagnostic imaging. Many patients imaged in small animal practice are small enough to fit both of these cavities within the boundaries of the radiographic detector, making acquiring these images possible in a way that it is not typical of radiography of humans. Such images theoretically provide some important advantages. They allow for a rapid appraisal of the entire patient, which can be particularly valuable for traumatic injuries and diseases that may affect both major body cavities, such as neoplasia. They should require less time to complete the needed examination compared to obtaining individual studies, which may be important for critically ill or fractious patients as well as to overall efficiency. Finally, gaining the same information from one study as opposed to two or more may be less expensive for clients, which will help control the expense of the entire course of treatment and diagnostics.

Whole-body projections are not without distinct limitations, however. Principle among these may be the different technique considerations for different anatomic regions of the patient. Subject contrast can vary greatly amongst the anatomic regions and body cavities of animal patients. Subject contrast refers to the differential transmission of x-ray radiation through different parts of a patient, and it provides the basic information that forms the radiograph. It is influenced by the thickness, density, and effective atomic number of the tissue imaged.<sup>1-3</sup> Differences in subject contrast create a requirement for differences in technique to form an optimum radiographic image. Subject contrast can

even differ greatly within a single anatomic region. The large amount of air contained within the lungs in the thorax yields a high subject contrast in this cavity. Very little air is present in the abdomen, and a much lower amount of inherent subject contrast is provided by the smaller contrast difference between the soft tissue abdominal viscera and the surrounding mesenteric fat. In addition, tissue thickness may vary greatly in an animal from the cranial thorax to the region of the last ribs and finally to the caudal abdomen. Any extremities included in the projections will have an even greater difference in thickness.

In screen-film radiography, such changes in subject contrast greatly complicate acquiring adequate whole-body projections. Each type of radiographic film possesses a specific “characteristic curve”—also known as an “H and D” or Hunter and Driffield curve—that is intrinsic to the film based on its construction. This curve describes the relationship between relative exposure of the film or screen-film system to x-ray radiation and resulting film density. For x-ray film, the curves have a sigmoid appearance with a fairly narrow region in which there is a linear response to different radiation doses. Exposures only a small amount above or below this narrow acceptable range result in non-diagnostic images. The slope of the linear region of the curve determines to what degree that film will amplify contrast in the resulting image. Because the curve is intrinsic to each individual film, the amount of contrast added by each kind of film is intrinsic to it and cannot be changed following image acquisition.<sup>1,2,4</sup>

Due to this property of x-ray film, radiographic technique must be carefully controlled to provide for diagnostic quality radiographic images in screen-film radiography. Precise technique charts are required to describe the changes in kiloVoltage peak (kVp) and milliAmpere seconds (mAs) needed to create an appropriately exposed radiograph at different body part thickness levels. These charts must be further specified for anatomic region (e.g. thorax, abdomen, extremity), the speed of the film-screen system being used, and the use or non-use of a grid. In addition, technique can also be affected by quality of electrical input from the x-ray generator, inherent differences in the x-ray machine, the

amount of beam filtration, and the age of any intensifying screens being used. Because of this, technique charts must be developed separately at each veterinary facility and ideally for each x-ray machine being used.<sup>5</sup> Finally, adjustment of kVp in film-screen radiography can provide for a radiograph with either high contrast or wide latitude; it is not possible to do both at the same time.<sup>3,4</sup> These technique limitations in screen-film radiography make it difficult to impossible to achieve a radiograph that is considered high quality for multiple anatomic regions, as is desired in whole-body radiography. Indeed, it can even be impossible to achieve the ideal exposure for sub-regions of one anatomic area. A wide latitude technique needed to properly evaluate the pulmonary parenchyma may not provide enough contrast for mediastinal structures, and proper high-contrast bone technique for extremities will limit visualization of the surrounding soft tissue.

The lack of collimation in whole-body radiography may cause issues beyond these technique concerns. Collimation is an essential step in radiography to limit the primary beam to the desired region of the patient's anatomy. This kind of beam restriction has two important functions: decrease of scatter radiation and protection of patient and personnel from radiographic exposure. In diagnostic radiography, almost all of this scatter radiation comes in the form of Compton scattering interactions. Photons from the primary beam strike electrons in the target material and are deflected in this interaction. These scattered photons can lower radiograph quality by striking the detector in an unexpected location following their deflection and can increase radiation dose to veterinary personnel by being deflected into those restraining the patient. Overall field size is an important factor in the amount of scatter radiation that reaches the x-ray detector. As the field size is increased, the amount of scatter radiation produced increases rapidly and then tapers until it hits an upper limit at a field size of 30 x 30 cm.<sup>1,2</sup> Scatter has an important effect on film quality, and collimation plays a role in this process. Radiographs in which the exposed portion of the film is limited by collimation are known to be of significantly higher quality than those in which the exposed portion of film is limited by lead shielding

placed directly adjacent to the film due to the effects of scatter, which are not limited by the lead shielding. In addition, films with the smallest collimation field are considered to be of the “highest technical quality,” due to the decreased production of scatter and centering of the beam on the area of interest.<sup>5</sup>

Appropriate collimation should also decrease the exposure to the patient as well as to any staff needed to restrain the patient by both decreasing the chance their hands will be within the primary beam and decreasing the overall scatter radiation produced to which they will necessarily be exposed by being in the room.<sup>5</sup> Proper radiation safety is an important consideration in the development and evaluation of any radiographic examination or procedure. The estimated yearly radiation dose for a medical worker is 0.1-3 mSv (10-300 mRem). This is lower than the maximum permissible dose of 50 mSv (5 Rem) per year set by the National Council on Radiation Protection and Measurements.<sup>6</sup> However, only limited information is known on the biological effects of exposure to low doses of radiation. This is especially true for consistent low exposures over a long term. Veterinary personnel are at a particular risk for this kind of exposure because almost all veterinary radiographic examinations require restraint of the patient during the examination, and this restraint is often performed manually by veterinary staff.<sup>7</sup> The acceptable level of radiation exposure to medical personnel and patients is governed by the principle of ALARA—As Low As Reasonably Achievable. This principle demands that any radiation exposure be avoided unless it provides a compelling benefit outweighing the risks of radiation, such as the diagnostic information gained from radiography. But even when a benefit is present, the ALARA principle requires the radiation dose to be minimized to whatever degree is possible.

Whole-body radiography necessarily involves less collimation, and therefore more scatter radiation will be produced in these examinations. This has implications for staff exposure as well as image quality. Whole-body radiography may even conceivably offer an advantage in decreasing radiation dose if the increase in scatter dose is small enough that the single whole-body radiograph

provides less exposure to personnel than the need for two separate regional studies to acquire the same information.

Due to these concerns, whole-body radiography is generally not in favor in the veterinary radiology community. The advent of digital radiography, however, has caused some significant changes in the factors contributing to obtaining quality radiographs. Digital detectors possess a much longer dynamic range than screen-film detectors. They preserve a linear response to a much wider distribution of radiation doses than does radiographic film, in which exposures above and below their narrow range result in non-diagnostic images.<sup>2,8</sup> While the dynamic range of screen-film systems is approximately 1:30, the dynamic range of digital detectors is often greater than 1:10,000.<sup>9</sup> Digital detectors are known to even have as much as a 400-fold greater linear response to radiation than film-screen systems.<sup>10</sup> In addition, following the exposure the associated computer system processes the raw digital image to both mimic the appearance of traditional screen-film radiography as well as to maximize the quality of the resulting displayed image. Modern digital systems typically utilize multi-scale image processing. In this technique, the image is transformed into multiple spatial frequency bands, and separate processing steps can be performed on each sub-region based on its unique qualities. High contrast regions can have their contrast lowered (latitude increased), and low contrast regions can have their contrast enhanced.<sup>9,11</sup> This is a significant improvement over screen-film radiography, in which technique settings or the kind of film selected can be chosen to provide a high contrast or high latitude image, but it is not possible to do both in different regions within the same image. Technique charts for digital system are therefore much more basic than those in film-screen radiography, with different settings often only needed to cover large ranges of patient thickness and the major anatomic regions.<sup>4</sup>

This processing is crucial, as it allows the display of regions with different contrast quality on one image, such as adequate exposure for both bone and surrounding soft tissue on an extremity radiograph. This was not previously possible with the limited dynamic range and lack of digital

processing in screen-film systems. Processing may further mitigate the effects of scatter in decreasing the contrast resolution of the resulting image. Though digital radiography is limited by its significantly lower spatial resolution than screen-film radiography, its greatly superior contrast resolution and multiscale processing have generally proved it to be superior or equivalent to screen-film systems in diagnostic performance.

Other factors not counteracted by digital radiography may still limit the diagnostic usefulness of whole-body radiography. Because radiography involves projection of a three dimensional structure into a two dimensional image from a primary beam diverging from a focal spot, geometry can play an important role in the appearance and diagnostic quality of the final image. In fact, problems of geometry are considered one of the most important causes for loss of radiographic detail.<sup>5</sup> Distortion of the shape of an object on a radiograph occurs when there is unequal magnification of different parts of the same object. This occurs when the object is not parallel to the plane of the film. For example, a very thin circular object that is tilted with respect to the plane of the film will have an elliptical shape on a radiograph. The end size and shape of this object will also vary depending on the position of the object within the x-ray beam as it diverges from the focal spot. For thick objects, which are commonly the kinds of objects found in patient anatomy, the problem is even more constant. Different parts of thick objects are different distances from the detector, so these objects will always undergo distortion unless they are directly in the central part of the x-ray beam. Finally, objects that are different distances from the film and outside of the central part of the x-ray beam may experience distortion of position. This occurs because the magnification of the distance between the object further from the detector and the midpoint of the image is greater than that for the object close to the detector. This unequal magnification may cause a distortion of the relative positions of the two objects on the radiograph. The least distortion therefore occurs with as much of the objects of interest in the center of the x-ray beam as possible. Whole-body radiography by necessity involves using a more divergent x-ray beam than

more specific region radiography, and thus makes it more likely that more important structures will be outside of the central part of the beam and subject to greater distortion. These distortion effects are not compensated for by digital radiography, and may still limit the diagnostic value of whole-body radiography.<sup>1,2</sup>

Factors specific to the presentation of a larger portion of the patient's anatomy may also affect the diagnostic accuracy of whole-body radiography. In human radiology, a phenomenon known as "satisfaction of search" has been described in which the presence of conspicuous lesions on an image lowers the ability to detect inconspicuous lesions.<sup>12</sup> The exact cause of this phenomenon is not known, as eye movement research has not shown that the attention of interpreters is so distracted by the obvious lesion that they spend significantly less time scanning the region with the inconspicuous lesion.<sup>13,14</sup> This may, however, apply an additional limitation in the value of whole-body radiographs in which whole body radiographs are used to attempt to combine evaluation of a known obvious lesions with a survey and search for subtle abnormalities of a separate cavity (e.g. whole body radiographs of an animal with a palpated large abdominal mass in which a search for pulmonary metastasis is also desired).

These changes have caused some veterinary radiologists to propose that whole-body radiography may now be an acceptable approach for many small dogs and cats, given the use of a high-quality digital system.<sup>15</sup> This argument is based on the idea that the major obstacles to obtaining appropriate whole-body radiographs are the technique changes mandated by differences in subject contrast between body cavities and the effects of scatter, and that these obstacles are eliminated or substantially reduced by the digital system with appropriate multiscale processing. Research is needed to determine if the advantages of digital radiography are enough to surmount the drawbacks of whole-body radiography.

The purpose of this study was to evaluate the image quality of collimated and whole-body radiographic projections of small animals. This was performed using visual grading analysis and visual grading characteristic analysis to grade the portrayal of normal thoracic anatomy by these two techniques. In addition, the effect of collimation on the amount of scatter radiation produced during radiography was assessed. The overall objective is to provide important initial information to guide selection of optimum techniques for digital radiography of small animal patients balancing image quality and radiation safety factors.



## II. Literature Review

### Digital Radiography

A variety of studies have suggested that digital radiography can replace traditional screen-film systems without loss of diagnostic accuracy or quality in various human clinical applications.<sup>16-30</sup> Several of these studies also supported the benefits of wide linear response and processing in digital radiography by showing that a significant dose reduction was possible without significant loss of image quality in the digital systems compared to a screen-film system. Fewer studies have been conducted in veterinary medicine, but these show a similar trend. In dogs, computed radiography has been found to be more sensitive for the detection of a small volume of pneumothorax compared to conventional radiography.<sup>31</sup> Digital radiography has also been found to have a similar degree of quality as film-screen radiography for orthopedic evaluation and measurements of the canine coxofemoral joints and tibial plateau angle.<sup>32-34</sup> Finally, a more general comparison of film-screen and digital radiography in portrayal of the thorax, abdomen, skull, femur, hip joints, elbow or the dogs found superior quality in the digital images.<sup>35</sup> High quality for digital images has also been found in feline chest radiography.<sup>36</sup> In horses, digital radiography has been found to increase subjective image quality relative to film-screen radiography.<sup>37,38</sup> Equine digital radiography has also shown higher accuracy in the diagnosis of subtle artificial lesions of the third metacarpal relative to film-screen radiography.<sup>39</sup> In other clinical veterinary applications, digital radiography has been validated as equivalent or superior to film-screen in birds<sup>40</sup> and snakes.<sup>41</sup> In research applications, digital radiography has also been validated in pigs,<sup>42</sup> rabbits,<sup>43</sup> and monkeys<sup>44</sup> as human models.

No studies have been conducted to assess the effects of collimation on image quality in either human or veterinary medicine. One veterinary study did evaluate the effect of digital multiscale processing on image quality in regards to scatter radiation. In this study, radiographs taken with no grid but with multiscale digital processing were found to be better than radiographs taken with a grid and without processing.<sup>9</sup> A grid is a device used to preferentially filter scatter radiation and prevent it from reaching the radiographic film or digital detector. Use of a grid results in an image with a high proportion of primary beam radiation to scatter radiation exposing the detector, and therefore improves quality by mitigating the deleterious effects of scatter radiation. The results of this study indicate that modern digital processing may be even better than grids at mitigating the negative effects of scatter radiation on image quality, which has implications for whole-body radiography.

One previous study from human medicine provides some evidence that digital radiography makes collimation a less important factor in image quality. In this study it was found that the amount of collimation used while obtaining lumbar radiographs was significantly reduced in two hospitals following a transition from screen-film to digital radiography.<sup>45</sup> This occurred despite these hospitals having no formal change in their protocol for lumbar imaging during this time. This decreased collimation may have been accepted by the radiographers at least in part because the digital system and its processing were able to compensate for the negative effects a wider field would have had on image quality.

### **Image Quality Comparison and Visual Grading Analysis**

Many methods have been developed to evaluate and compare the performance of diagnostic imaging systems.<sup>46</sup> These methods are necessary to help determine the diagnostic quality of an imaging procedure and to evaluate new imaging technologies and approaches to assure that they are equivalent or superior to existing ones. Some of these methods rely on specific physical measurements, such as

calculation of the detective quantum efficiency (DQE), modulation transfer function (MTF), or signal-to-noise ratio (SNR). Though these standards provide objective means to compare imaging systems, they evaluate the image based on standards that may be significantly different from that of the human observer and fail to take into account the effect of the displayed anatomical background on proper image interpretation. A different group of methods attempts to approach these evaluations at the level of the end observer by asking observers to assess the visibility of certain features of the image. The benefit of these approaches is that they evaluate the imaging system at the level of most clinical importance—the end observer—and thus take into account all components in the imaging chain. The most traditional of these methods is Receiver Operating Characteristic or ROC analysis. ROC analysis is meant to evaluate the fundamental task of diagnostic imaging in characterizing the patient as normal or abnormal. It was developed due to the limitations in applying the more common tools used to evaluate and compare the accuracy of diagnostic tests, such as sensitivity and specificity, to diagnostic imaging procedures due to the involvement of an observer in diagnostic imaging. For an observer, changes in sensitivity and specificity are closely tied to changes in the decision threshold; an observer who decides to use a stringent decision threshold to avoid false positives will be increasing specificity at the cost of reduced sensitivity. Because large inter- and intra-observer variance can be present for diagnostic imaging tests, sensitivity and specificity do not provide all of the information needed to adequately compare the diagnostic accuracy of these tests. ROC analysis can be used to get around this problem by plotting all possible compromises between the true positive and false positive rates, meaning all possible different decision thresholds. Thus it is the inherent accuracy of the different diagnostic tests, and not the different decision thresholds of different observers, that are compared in ROC analysis.<sup>46,47</sup> Although ROC analysis provides a powerful tool for comparing the performance of diagnostic tests such as different imaging approaches, it has some disadvantages as well. Proper ROC analysis requires using cases either with lesions confirmed through some gold standard reference or phantom lesions

painstakingly created on normal controls to appropriately mimic real cases.<sup>46,48-49</sup> Also, the most basic kind of ROC analysis, in which the observer is merely asked to classify each case as normal or abnormal, is vulnerable to situations in which the observer both misses the actual lesion and incorrectly detects a lesion on a different portion of the image. In this situation the observer has actually made two separate mistakes, but they will cancel and falsely increase the accuracy of the diagnostic test being used. This can be compensated for by newer techniques in ROC analysis which involve “free-response” or localization specific evaluation, but this only increases the time-consuming nature of these studies and the complexity of the resulting statistical analysis.<sup>46</sup> ROC analysis also almost always involves observers who are not blinded to their participation in a study. There is therefore some concern about generalizing these studies, as this knowledge of participation in the study appears to have an effect on how the observers evaluate the final images, although the magnitude of the effect is not completely clear at this time.<sup>49-50</sup> Finally, the need for the observer to come to a conclusion about each image also increases the amount of work and time that must go into each study.

For these reasons, ROC studies may not be the ideal for more basic comparisons between imaging approaches, such as alterations in technique, the use of a different grids, or the amount of collimation used. A different technique, known as visual grading, has been developed to provide a simpler means of comparing variations in diagnostic imaging approaches. Visual grading studies involve observers evaluating how well an imaging study portrays certain components of a subject’s normal anatomy.<sup>46-47,51</sup> Much like ROC analysis, these studies should offer high practical validity by taking into account all components in the imaging chain, including the response of the end-observer to the image. They further emerge from one of the central assumptions of diagnostic imaging: that detection of pathologic lesions is dependent on proper reproduction of anatomy. Because these lesions represent variations from the normal anatomy, they should be most visible when the patient’s anatomy can be most clearly seen and evaluated. Therefore the imaging approach that best reproduces the patient’s

anatomy should provide the greatest diagnostic value. The validity of this assumption is supported by studies showing agreement between visual grading and both ROC<sup>52-53</sup> and physical calculations of image quality.<sup>54-56</sup> Research has also indicated the importance of the patient anatomy in lesion identification. In human patients the detection of small pulmonary nodules, defined as less than 10mm in diameter, was found to be far more influenced by the patient's anatomy than by the noise in the radiographic image.<sup>57</sup> In addition, the greatest advantage of visual grading studies over other approaches may actually be the ease of applying this kind of study. The workload in both preparing and participating in these studies is significantly less than in ROC analysis.<sup>46,58</sup> The time commitment for the participating radiologist is typically only a few hours. In comparison, many ROC studies are so time consuming that they must be spread over several months to give participants enough time to complete their responses.<sup>49</sup>

Other studies have suggested some qualifications concerning the overall validity of visual grading analysis as a measure of the clinical utility of an imaging approach. A study in lumbar spinal radiographs found that image quality decreased as exposure dose increased—and thus image noise increased—as expected. But an ROC study of artificial lesions did not find a similar decrease in diagnostic accuracy.<sup>59</sup> Thus lesion conspicuity did not have a strong relation to subjective image quality. In another study of image processing algorithms in digital mammography, visual grading analysis was found to be discordant from ROC results.<sup>58</sup> These results suggest that ROC remains the gold-standard result for validating the overall clinical utility of an imaging approach, and therefore that adequate portrayal of normal anatomy is a necessary but not sufficient component of the overall diagnostic performance of an imaging procedure. Finally, a study in computed tomography found that the observers gave significantly lower grades to one protocol with a very low dose rate, even though more objective physical calculations of contrast-to-noise ratio and signal-to-noise ratio did not find a significant difference.<sup>60</sup> This corresponded to the results from the lumbar spine study, in that noise may

have a significant effect on subjective quality of portrayal of normal anatomic structures, but this will not necessarily diminish visualization of clinically important lesions.

Two different methods of visual grading studies have been developed. The first, known as an image criteria (IC) study, involves the observer indicating whether or not the presented image meets a certain set of criteria. As is evident, such a study requires that criteria be available for the imaging examination of interest. In human medicine, the European quality criteria are available for the standard adult and pediatric radiographic and computed tomographic examinations.<sup>61-63</sup> These criteria were developed by an international panel of radiologists and physicists and provide a ready tool for IC and other visual grading studies. They provide guidance both of the proper positioning of the examination and the needed level of reproduction for important anatomic structures in each examination. An example of the criteria for chest radiography is presented in tables 1-2. After the observer indicates whether the criteria were fulfilled or not in the presented image, an image criteria score (ICS) can be calculated as the proportion of criteria that were fulfilled. Because this score is developed based on a binary decision, the use of parametric statistics is valid for this kind of study. This is one of the chief advantages of the IC approach, and it is also likely the easiest and least cumbersome of the visual grading techniques. IC has a disadvantage in requiring the observer to make a binary decision rather than allowing a range of possible responses that may allow them to more accurately convey their evaluation of the quality of the presented image. Unfortunately, no current standardized criteria for quality radiographs exist in veterinary medicine. However, existing references do provide guidance as to the typical standards for a quality radiographic examination in veterinarian patients from which appropriate criteria may be derived.<sup>64,65</sup>

**Table 1. European quality criteria for posterior-anterior (PA) chest radiographs in humans.**<sup>61</sup>

<b>1. DIAGNOSTIC REQUIREMENTS</b>
<b>1.1. Image criteria</b>
1.1.1. Performed at full inspiration (as assessed by the position of the ribs above the diaphragm — either 6 anteriorly or 10 posteriorly) and with suspended respiration
1.1.2. Symmetrical reproduction of the thorax as shown by central position of the spinous process between the medial ends of the clavicles
1.1.3. Medial border of the scapulae to be outside the lung fields
1.1.4. Reproduction of the whole rib cage above the diaphragm
1.1.5. Visually sharp reproduction of the vascular pattern in the whole lung, particularly the peripheral vessels
1.1.6. Visually sharp reproduction of: (a) the trachea and proximal bronchi, (b) the borders of the heart and aorta, (c) the diaphragm and lateral costo-phrenic angles
1.1.7. Visualization of the retrocardiac lung and the mediastinum
1.1.8. Visualization of the spine through the heart shadow
<b>1.2. Important image details</b>
1.2.1. Small round details in the whole lung, including the retrocardiac areas: high contrast: 0.7 mm diameter low contrast: 2 mm diameter
1.2.2. Linear and reticular details out to the lung periphery: high contrast: 0.3 mm in width, low contrast: 2 mm in width

**Table 2. European quality criteria for lateral chest radiographs in humans.**<sup>61</sup>

<b>1. DIAGNOSTIC REQUIREMENTS</b>
<b>1.1. Image criteria</b>
1.1.1. Performed at full inspiration and with suspended respiration
1.1.2. Arms should be raised clear of the thorax
1.1.3. Superimposition of the posterior lung borders
1.1.4. Reproduction of the trachea
1.1.5. Reproduction of the costo-phrenic angles
1.1.6. Visually sharp reproduction of the posterior border of the heart, the aorta, mediastinum, diaphragm, sternum and thoracic spine
<b>1.2. Important image details</b>
1.2.1. Small round details in the whole lung: high contrast: 0.7 mm diameter low contrast: 2 mm diameter
1.2.2. Linear and reticular details out to the lung periphery: high contrast: 0.3 mm in width low contrast: 2 mm in width

The second major visual grading approach, known as visual grading analysis (VGA), involves observers evaluating image quality using a multi-step scale rather than as a binary decision about whether the criteria were fulfilled or not. This greater freedom should allow the observer to more accurately state their evaluation of the quality of the key structures in the presented image. VGA studies can be split further into relative and absolute studies. In relative studies, reference images are provided, and observers then compare the study images to these and evaluate structures as better than, equivalent to, or worse than the reference images, usually with a scale of possible ratings provided to them. In absolute studies, no reference images are provided, and observers must rank structures on the study images based on an absolute scale, also ideally provided by the study designers. Though VGA

studies provide more freedom in evaluating the quality of images, there are complications in the proper statistical analysis of the results. Because the steps in the multi-step scales used in these studies are assigned a numerical value, some VGA studies have involved the calculation of a visual grading analysis score (VGAS), which is typically the mean value of all of the ratings for that image. The purported advantage of this approach is ease of comparing different images both directly and through statistical tests such as analysis of variance (ANOVA). However, the VGA ratings represent ordinal values that are not quantitative integral values. The use of VGAS therefore has neither statistical nor mathematical validity. Instead, the rankings created in a VGA study must be compared using either non-parametric tests or visual grading characteristics (VGC) analysis. VGC analysis treats the VGA ratings in a manner similar to ROC analysis, generating a curve that can be used in a statistically valid comparison of different imaging approaches. In addition to being statistically valid, this test follows the assumptions underlying ROC analysis, therefore allowing software packages for ROC analysis to be used for VGC analysis. VGC analysis further provides a number value, the area under the curve ( $AUC_{VGC}$ ) which can be used to compare different diagnostic imaging approaches. An  $AUC_{VGC}$  of 0.5 indicates that there is no difference in imaging quality between the test being studied and the reference test. An  $AUC_{VGC}$  of greater than 0.5 indicates the new test provides superior quality, while an  $AUC_{VGC}$  of less than 0.5 indicates that the reference test is superior.<sup>48,51</sup>

Because they rely on subjective evaluation of images of otherwise normal patients, VGA studies have been criticized as a “beauty contest.”<sup>46,66</sup> The concern is that observers will evaluate the images based on irrelevant criteria or will be biased based on personal familiarity and comfort. In one VGA study of different screen-film combinations in human portable chest radiography, the observers, who were drawn from multiple hospitals, were found to prefer whatever combination was in use in their own hospital at that time. They were therefore picking not the image that they necessarily evaluated as the highest quality reproduction of the pertinent anatomy, but rather the one that looked the most similar



to the studies they typically evaluated in their daily jobs.<sup>67</sup> Crucially, the observers in this study were not given any criteria to use or other guidance in rating the images. This indicates the importance of providing appropriate criteria in these studies, a task complicated in veterinary medicine by the lack of previously agreed upon imaging criteria.

VGC studies have been successfully performed in both human and veterinary radiology. In veterinary radiology, VGA and VGC analysis has been applied to investigations of the effect different storage phosphor types have on image quality in feline chest radiography, finding that phosphors with a needle-type architecture produced superior image quality to conventional phosphors, and the continued to be superior even at a reduced dose.<sup>68</sup> Another study used VGC to evaluate the effect of monitor type on image quality, finding that medical grade grayscale monitors had superior performance to consumer-grade color monitors, and that the color cathode ray tube monitor outperformed the color liquid crystal display monitor.<sup>69</sup> A third veterinary study used VGA in comparing digital and film-screen systems in avian radiography. In this study no significant difference was found between digital and film-screen radiography for most criteria, and in a few criteria the digital system was significantly better than the film-screen.<sup>40</sup> In these three studies VGA was found to be a useful and practical means for comparing image quality between different approaches at different levels of the imaging chain.

In human radiology, VGA has been used in a more diverse body of studies. The major focus of these studies have been optimizing patient dose in x-ray based imaging (radiography and computed tomography). In radiography, VGA studies have been used to optimize dose and quality in lumbar spinal radiographs,<sup>70</sup> in double contrast barium enema examinations,<sup>71</sup> in digital mammography,<sup>58</sup> to evaluate dose reduction<sup>72</sup> and how image processing can help optimize dose while maintaining quality in pediatric radiology,<sup>73</sup> and in optimizing tube voltage in conventional urography using a digital detector.<sup>74</sup> Computed tomography studies have been performed to determine if post-processing filtration allows reduction dose rate for abdominal CT<sup>75</sup> and using different processing approaches and in optimizing CT

and intravenous contrast dose for patients in various age ranges.<sup>60</sup> VGA and VGC techniques have also been used in magnetic resonance imaging to compare MRI sequences in optic bulb volumetry,<sup>76</sup> in detecting edema in breast-MR,<sup>77</sup> and in 2D and 3D functional MRI.<sup>78</sup>

### **Radiation Safety and Scatter Radiation**

A limited number of studies have been undertaken on radiation safety practices at veterinary facilities, and these studies give reason for concern about improving veterinary radiation safety. The earliest studies painted a bleak picture of initial safety practices in veterinary medicine. A 1964 study of protective practices among veterinarians in Michigan uncovered many safety hazards including 82% of practices with inadequate filtration on their x-ray machines, 18% with no lead aprons available for staff, 25 illegal fluoroscopes still in use, and perhaps most pertinent for the current topic 75% of practices using excessive primary beam field size. Very few practices were noted to use film badges to record the exposure of their staff over time. Most alarmingly, the group of veterinarians studied here were found to be aware of the dangers to radiation exposure, but many failed to exercise appropriate precautions or even follow state regulations on radiation safety.<sup>79</sup> An earlier 1957 study found that personnel at one quarter of facilities inspected did not use leaded protective equipment even though it was available and one fifth of the practices lacked any external beam limiting device. This study also confirmed the danger a lack of limiting field size could pose by showing that the radiation dose from scatter with the beam limiting device (a cone at this point in time) was 3-5 mR/s while the radiation dose from scatter with no beam limiting device was ten times higher at 30-50 mR/s.<sup>80</sup> A 1970 survey of 41 veterinarians and veterinary personnel found 75% had chronic radiation burns to their hands.<sup>81</sup> These poor practices contributed to an epidemiologic study of mortality in veterinarians from 1947-1977 which found a

significant increase in the number of deaths from leukemia during the period where the use of radiographic procedures became more common but in which proper protective procedures were rarely followed.<sup>82</sup>

More recent studies suggest improvement in safety practices but a corresponding increase in the quantity of radiographic procedures performed. Both a 1989<sup>83</sup> and a 2000<sup>84</sup> study found an increase in the percentage of veterinarians wearing appropriate protective equipment during radiographic procedures as well as an increase in the number of radiographic procedures occurring and the percentage of veterinarians participating in these procedures. This indicates that while positive changes in safety have been occurring, the increased importance of radiographic procedures in the veterinary diagnostic workup may still lead to excessive radiation doses to personnel if every possible step is not employed to limit exposure.

Though studies have been conducted on the effect of kVp on scatter dose<sup>85</sup> as well as the early research confirming an increased scatter dose when no beam limitation was used discussed above,<sup>86</sup> no study has been conducted comparing the radiation dose for a standard regional examination with the less collimated whole-body examination.

### III. Materials and Methods

33 privately owned small dogs were recruited for use in this study. All dogs measured less than 43 cm (approximately 17 inches) in length from the point of the shoulder joint to the greater trochanter of the femur and ranged in age from one to seven years. All dogs received an initial physical examination, and their weight, body condition score, length, width (from lateral to lateral), and thickness (from ventral to dorsal) were recorded. Two of the dogs were excluded from the study due to abnormalities found on their initial physical examination, both due to the presence of a heart murmur on thoracic auscultation. There were no significant findings on the physical examination of the remaining dogs pertinent to this study.

Four radiographic projections were obtained for each dog. The dogs were positioned in right lateral recumbency for right lateral projections and in dorsal recumbency for ventrodorsal projections. For each positioning a projection collimated so that the primary beam contained only the thoracic cavity as well as a non-collimated whole-body projection containing the patient's entire torso were obtained (Fig. 1). Patients were restrained using typical techniques for clinical radiographic imaging of dogs, including the use of pads and padded troughs as well as manual restraint. Projections were repeated as needed for positioning.

All projections were obtained in the same radiography room using the same equipment. A Varian Rad-14 x-ray tube with a Transworld 625V x-ray generator was used. The same technique was used for all projections, with a small focal spot size (0.6mm), 80 kVp, and 3.33 mAs (400 mA x 8.33 ms). Collimation was performed using a Machlett Coll-M 150 collimator. Images were detected and acquired

by an Eklin DR6 direct digital radiography system with a Canon CXDI-50G detector plate. The same standard thoracic processing algorithm was used for all images.

The four acquired projections for each patient were then exported as non-compressed TIFF images. These images were then cropped to portray just the thoracic anatomy using a digital image editing software (GNU Image Manipulation Project (GIMP)). The collimated images were minimally cropped to remove any small amount of excess anatomy, any visible borders from the edge of the primary field, and any other extra-thoracic features that might help identify the image to the blinded observer. The whole-body projections were cropped to include just the thorax. Care was taken to match the anatomic area and pixel size of the resulting images for each patient in the cropped versions of the collimated and whole-body projections (Fig. 2). In general, the cropped images extended from C7 to T12. The cropped images were then assigned a random number.

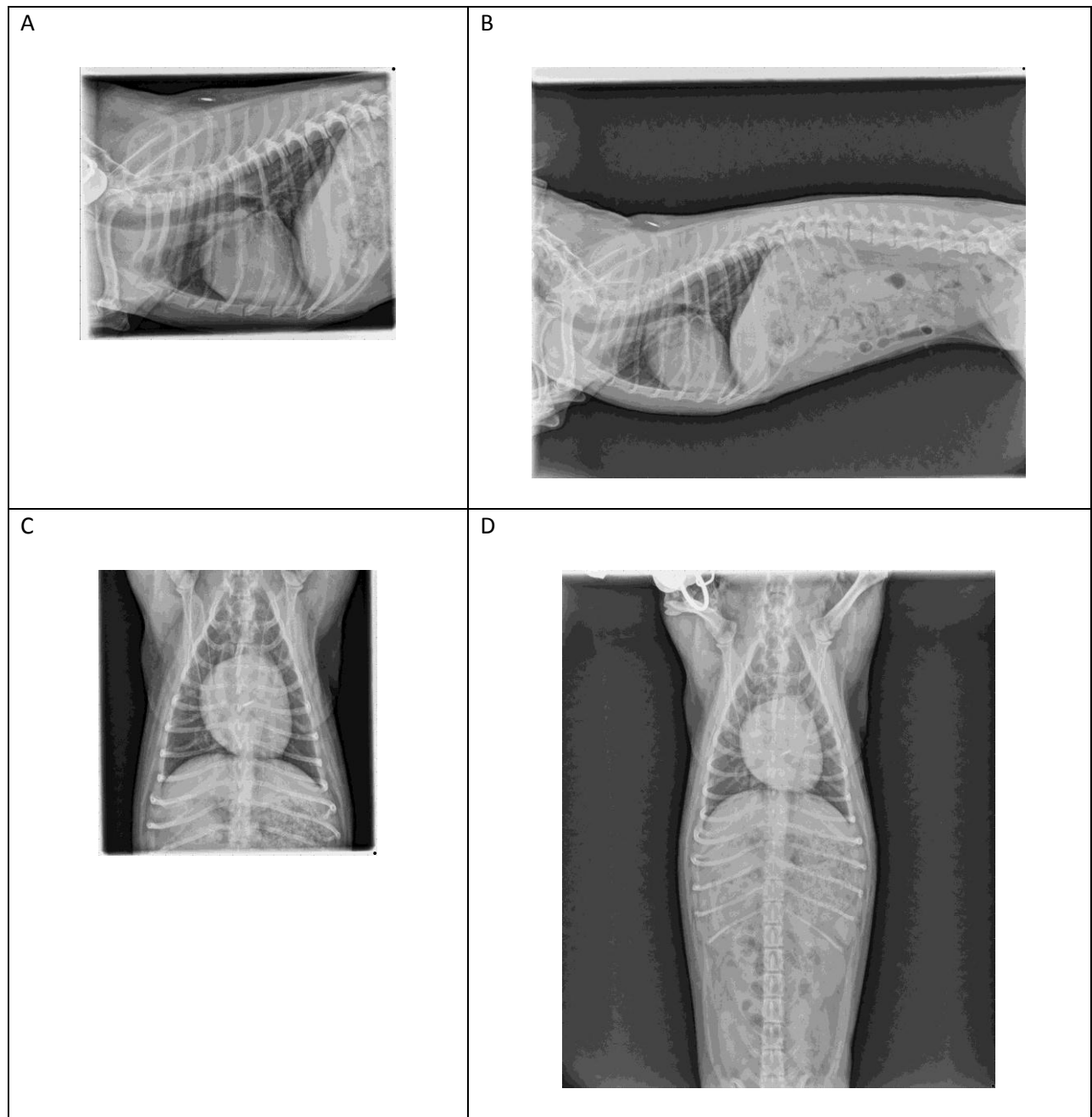
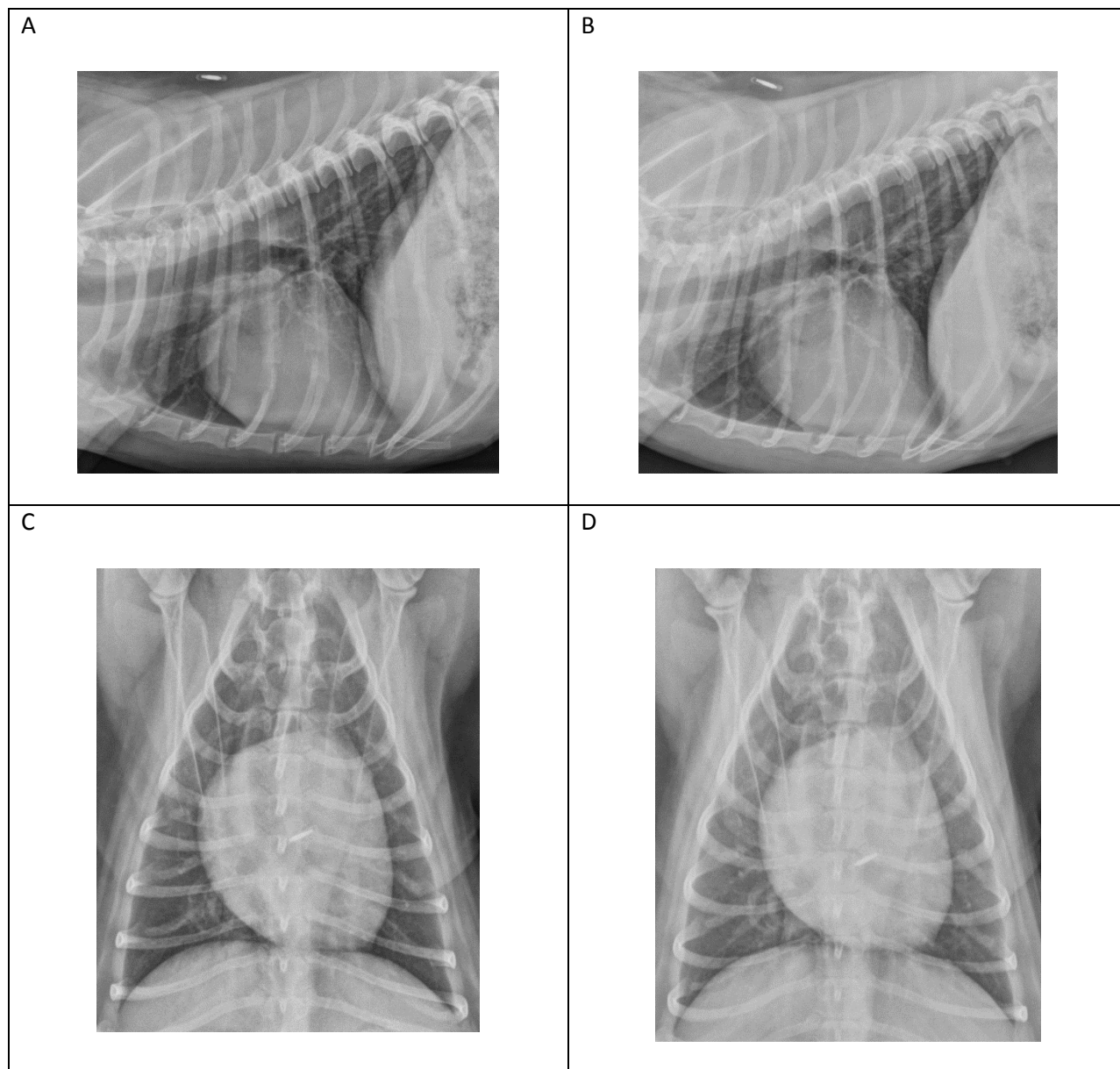


Figure 1. Initial uncropped (A) collimated lateral, (B) whole-body lateral, (C) collimated ventrodorsal, and (D) whole-body ventrodorsal projections for one of the subjects.



**Figure 2. Final images from the same case as in figure 1 after digital cropping. These images were initially the A) collimated lateral, (B) whole-body lateral, (C) collimated ventrodorsal, and (D) whole-body ventrodorsal projections. These cropped images were randomized and evaluated by the blinded radiologists in the study.**

These randomized images were assessed by five veterinary radiologists, all with multiple years of experience interpreting digital radiographs. These radiologists were blinded to the imaging procedure used for each of the randomized images. The images were viewed on one of two diagnostic workstations using identical medical grade grayscale monitors (WIDE Model PGL21/IF2103A, 21 inch

diagonal length, 1536x2048 resolution, pixel pitch 0.207 x 0.207, brightness 800 cd/m<sup>2</sup>). Observers had unlimited time to view and grade each image.

Image quality was assessed using absolute visual grading analysis. Observers were asked to grade overall image quality on a five-step scoring system and to grade the portrayal of several anatomic structures using a three-step scoring system (**Table 3**). For lateral projections, observers assessed the cranial pulmonary vasculature, the caudal pulmonary vasculature, the trachea, the caudal mainstem bronchi, the heart and great vessels, and the ribs. For the ventrodorsal projections, observers assessed the caudal pulmonary vasculature, the trachea, the caudal mainstem bronchi, the heart, the caudal vena cava, the aorta, and the spine (**Table 4**).

**Table 3. Grades for the overall image quality (scale of 1-5) and for the individual anatomic structures (scale of 1-3)**

<b>Grade</b>	<b>Overall Image Quality</b>
1	<i>Poor image quality, loss of information and image not acceptable for clinical use.</i>
2	<i>Restricted image quality, loss of information and clinically relevant limitations</i>
3	<i>Adequate image quality, moderate limitations for clinical use</i>
4	<i>Good image quality, minimal limitations for clinical use</i>
5	<i>Excellent image quality, no limitations for clinical use.</i>
<b>Grade</b>	<b>Anatomic Structures</b>
1	<i>Structure not visible and/or complete evaluation not possible</i>
2	<i>Structure visible but evaluation limited.</i>
3	<i>Structure clearly visible, complete evaluation possible</i>



**Table 4. Individual anatomic structures evaluated on the lateral and ventrodorsal projections and the corresponding criteria for evaluation.**

<b>Anatomic Structure</b>	<b>Criteria</b>
<b>LATERAL</b>	
<b>Cranial Pulmonary Vasculature</b>	Visually sharp reproduction of the cranial pulmonary lobar artery and vein
<b>Caudal Pulmonary Vasculature</b>	Visually sharp reproduction of the pulmonary vasculature in the caudal lung field
<b>Trachea</b>	Visually sharp reproduction of the tracheal borders.
<b>Caudal Bronchi</b>	Visualization of the origin of the caudal mainstem bronchi at the carina
<b>Heart</b>	Visually sharp reproduction of the borders of the cardiac silhouette and the great vessels (aorta and caudal vena cava)
<b>Ribs</b>	Visually sharp reproduction of rib borders
<b>VENTRODORSAL</b>	
<b>Caudal Pulmonary Vasculature</b>	Visually sharp reproduction of the pulmonary vasculature in the caudal lung field.
<b>Trachea</b>	Visualization of the trachea and its course to the carina.
<b>Caudal Bronchi</b>	Visualization of the origin of the caudal mainstem bronchi at the carina.
<b>Heart</b>	Heart is centered within the thoracic cavity with clear borders.
<b>CdVC</b>	Visually sharp reproduction of the caudal vena cava.
<b>Aorta</b>	Visually sharp reproduction of left lateral border of descending aorta overlying cardiac silhouette.
<b>Spine</b>	Visualization of the spine and spinous processes.

Statistical analysis was performed using open source and commercial statistical software.\*

Because the grades represented non-parametric data with a variable scale, interobserver variability was evaluated using Spearman’s rank correlation. Observer grades for the collimated and whole-body approach for each image were compared using the Wilcoxon Signed-Rank test. In addition, visual grading characteristic curves and areas under the curve ( $AUC_{VGC}$ ) and 95% confidence intervals were calculated, and the  $AUC_{VGC}$  data for the different observers for each criterion was compared using Forest plots . Histograms and descriptive statistics for the grayscale composition for each image were obtained using open source image analysis software.†

During the radiographic image acquisition, an ionization-chamber radiation detector‡ was placed in a standardized position at the same level of the patient and centered on the center of the primary field. This position correlated with the location of radiographic personnel restraining the patient during

\* Deducer, [www.deducer.org](http://www.deducer.org); MedCalc version 12.7, MedCalc Software, Ostend, Belgium

† ImageJ, US National Institutes of Health, Bethesda, MD, <http://rsb.info.nih.gov/ij/>

‡ Keithley Model 36150, Keithley Instruments, Solon, OH

imaging. The scatter radiation detected from each exposure was recorded. Mean scatter radiation for collimated and whole-body projections of each position were determined. These means were compared using the paired student's t-test.

## IV. Results

For the 31 dogs included in the study, the mean weight was 7.77 kg (range 2.0-22.7 kg). Median weight was 6.2kg. 25 of the cases (80.6%) had ideal body condition and six of the cases (19.4%) had elevated body condition scores. Mean length was 30.0 cm (range 17.75-43.0cm), mean width was 13.98 cm (9.0-24.5cm), and mean thickness was 16.27cm (range 10.0-25.0cm).

### Image Quality

The five blinded observers evaluated four de-identified and cropped images for each of the 31 subjects. There were 4,650 individual ratings compared in this study. The correlation in rankings for each criteria varied between observers (**Table 5, 6**). In 48 observer-criterion pairs correlation could not be calculated due to lack of variance in the grades given by one of the observers. There was generally poor correlation between observer 2 and all other observers on the grades for the lateral images. There was also poor correlation between observer 4 and all other observers for the grades for the ventrodorsal images. Observers 1, 3, and 5 had moderate to strong correlation in most of their grades across both lateral and ventrodorsal images. Observer 4 had at least moderate correlation with observers 1, 3, and 5 on the majority of the ratings for the lateral images, but had poor correlation with all other observers on the ventrodorsal images. Observer 2 had overall poor correlation with all other observers on the lateral images, but had significant correlation with observers 1, 3, and 5 on almost half of the ratings for the ventrodorsal images. Observer 2 overall gave higher grades for both individual anatomic structures and the overall image quality than the other observers, contributing to the decreased correlation with the

other observers. Overall, there was significant correlation on 102 of the 252 (41.3%) total observer criteria pairs that could be compared.

**Table 5. Spearman rank correlations of the grades for each observer pair for each criteria for the collimated and whole-body lateral images.**

<b>Lateral</b>						
<b>Collimated</b>	<b>Obs 1 : Obs3</b>	<b>Obs1 : Obs2</b>	<b>Obs2 : Obs3</b>	<b>Obs1 : Obs4</b>	<b>Obs2 : Obs4</b>	<b>Obs3 : Obs4</b>
Cranial Pulmonary Vasculature	0.4561 ( <i>p</i> =0.0099)	0.4423 ( <i>p</i> =0.0127)	0.05929 ( <i>p</i> =0.7514)	0.4936 ( <i>p</i> =0.0048)	0.5315 ( <i>p</i> =0.0021)	0.4101 ( <i>p</i> =0.0220)
Caudal Pulmonary Vasculature	0.4027 ( <i>p</i> =0.0247)	0.2978 ( <i>p</i> =0.1038)	0.3461 ( <i>p</i> =0.0565)	0.3669 ( <i>p</i> =0.0423)	(0.02085) ( <i>p</i> =0.9113)	0.2724 ( <i>p</i> =0.1381)
Trachea	0.5018 ( <i>p</i> =0.0040)	X	X	0.2128 ( <i>p</i> =0.2504)	X	0.03742 ( <i>p</i> =0.8416)
Caudal Bronchi	0.1419 ( <i>p</i> =0.4463)	(0.2462)( <i>p</i> =0.1819)	(0.08006) ( <i>p</i> =0.6685)	0.2682 ( <i>p</i> =0.1447)	0.2462 ( <i>p</i> =0.1819)	0.408 ( <i>p</i> =0.0227)
Heart	(0.1098) ( <i>p</i> =0.5565)	0.3246 ( <i>p</i> =0.0748)	0.2906 ( <i>p</i> =0.1059)	0.4089 ( <i>p</i> =0.0224)	(0.1287) ( <i>p</i> =0.4904)	0.055 ( <i>p</i> =0.7689)
Ribs	0.2651 ( <i>p</i> =0.1495)	X	X	0.2196 ( <i>p</i> =0.2353)	X	0.5353 ( <i>p</i> =0.0019)
Overall	0.4297 ( <i>p</i> =0.0178)	0.2768 ( <i>p</i> =0.1317)	0.1117 ( <i>p</i> =0.5497)	0.3835 ( <i>p</i> =0.0332)	0.1463 ( <i>p</i> =0.4321)	0.359 ( <i>p</i> =0.0275)
<b>Whole-Body</b>	<b>Obs1 : Obs3</b>	<b>Obs1 : Obs2</b>	<b>Obs2 : Obs3</b>	<b>Obs1 : Obs4</b>	<b>Obs2 : Obs4</b>	<b>Obs3 : Obs4</b>
Cranial Pulmonary Vasculature	0.586 ( <i>P</i> =0.0007)	0.2174 ( <i>p</i> =0.2401)	0.1989 ( <i>p</i> =0.2834)	0.4367 ( <i>p</i> =0.0140)	0.3561 ( <i>p</i> =0.0493)	0.6019 ( <i>p</i> =0.0003)
Caudal Pulmonary Vasculature	0.5508 ( <i>p</i> =0.0016)	0.2376 ( <i>p</i> =0.1980)	0.4433 (0.0125)	0.4726 ( <i>p</i> =0.0073)	0.2641 ( <i>p</i> =0.1511)	0.6722 ( <i>p</i> =0.0000)
Trachea	0.4171 ( <i>p</i> =0.0219)	X	X	0.3983 ( <i>p</i> =0.0265)	X	0.4778 ( <i>p</i> =0.0066)
Caudal Bronchi	0.1127 ( <i>p</i> =0.5532)	0.08494 ( <i>p</i> =0.6496)	0.3096 ( <i>p</i> =0.0901)	0.3963 ( <i>p</i> =0.0273)	0.2012 ( <i>p</i> =0.2778)	0.5018 ( <i>p</i> =0.0040)
Heart	0.254 ( <i>p</i> =0.1757)	0.0163 ( <i>p</i> =0.9307)	0.1213 ( <i>p</i> =0.5156)	0.3886 ( <i>p</i> =0.0308)	0.008476 ( <i>p</i> =0.9639)	0.3762 ( <i>p</i> =0.0370)
Ribs	0.5734 ( <i>p</i> =0.0009)	X	X	0.1746 ( <i>p</i> =0.3476)	X	0.6161 ( <i>p</i> =0.0002)
Overall	0.4914 <i>p</i> =(0.0058)	0.1933 ( <i>p</i> =0.2976)	0.2246 ( <i>p</i> =0.2244)	0.3751 ( <i>p</i> =0.0376)	0.5046 ( <i>p</i> =0.0038)	0.4085 ( <i>p</i> =0.0225)

Table 5 (continued)

<b>Lateral</b>				
<b>Collimated</b>	<b>Obs1 : Obs5</b>	<b>Obs2 : Obs5</b>	<b>Obs3 : Obs5</b>	<b>Obs4 : Obs5</b>
Cranial Pulmonary Vasculature	0.5655 ( <i>p</i> =0.0009)	0.534 ( <i>p</i> =0.0020)	0.3925 ( <i>p</i> =0.0290)	0.4969 ( <i>p</i> =0.0045)
Caudal Pulmonary Vasculature	0.4474 ( <i>p</i> =0.0116)	0.2238 ( <i>p</i> =0.2261)	0.243 ( <i>p</i> =0.1878)	0.6228 ( <i>p</i> =0.0002)
Trachea	X	X	X	X
Caudal Bronchi	0.3599 ( <i>p</i> =0.0467)	X	X	X
Heart	0.3599 ( <i>p</i> =0.0467)	0.1389 ( <i>p</i> =0.4562)	0.6823 ( <i>p</i> <0.0001)	0.055 ( <i>p</i> =0.7689)
Ribs	0.04192 ( <i>p</i> =0.8228)	0.2409 ( <i>p</i> =0.1917)	X	0.392 ( <i>p</i> =0.0292)
Overall	0.6623 ( <i>p</i> <0.0001)	0.5797 ( <i>p</i> =0.0006)	0.3383 ( <i>p</i> =0.0626)	0.4894 ( <i>p</i> =0.0052)
<b>Whole-Body</b>	<b>Obs1 : Obs3</b>	<b>Obs1 : Obs2</b>	<b>Obs2 : Obs3</b>	<b>Obs1 : Obs4</b>
Cranial Pulmonary Vasculature	0.3869 ( <i>p</i> =0.0315)	0.4047 ( <i>p</i> =0.0239)	0.4515 ( <i>p</i> =0.0108)	0.405 ( <i>p</i> =0.0238)
Caudal Pulmonary Vasculature	0.07914 ( <i>p</i> =0.6722)	0.3188 ( <i>p</i> =0.0805)	0.0753 ( <i>p</i> =0.6872)	0.1765 ( <i>p</i> =0.3421)
Trachea	0.1879 ( <i>p</i> =0.3115)	0.02117 ( <i>p</i> =0.9100)	X	0.1641 ( <i>p</i> =0.3779)
Caudal Bronchi	0.08494 ( <i>p</i> =0.6496)	0.3096 ( <i>p</i> =0.0901)	(0.03333) ( <i>p</i> =0.8587)	0.2012 ( <i>p</i> =0.2778)
Heart	0.2837 ( <i>p</i> =0.1219)	0.2263 ( <i>p</i> =0.2209)	0.2037 ( <i>p</i> =0.2717)	0.3426 ( <i>p</i> =0.0592)
Ribs	0.2005 ( <i>p</i> =0.2794)	0.3727 ( <i>p</i> =0.0389)	X	(0.0629) ( <i>p</i> =0.7367)
Overall	0.5989 ( <i>p</i> =0.0004)	0.5931 ( <i>p</i> =0.0004)	0.3651 ( <i>p</i> =0.0434)	0.704 ( <i>p</i> <0.0001)

Table 6. Spearman rank correlations of the grades for each observer pair for each criteria for the collimated and whole-body ventrodorsal images. Significant correlation is italicized.

<b>Ventrodorsal</b>						
<b>Collimated</b>	<b>Obs1 : Obs3</b>	<b>Obs1 : Obs2</b>	<b>Obs2 : Obs3</b>	<b>Obs1 : Obs4</b>	<b>Obs2 : Obs4</b>	<b>Obs3 : Obs4</b>
Caudal Pulmonary Vasculature	<i>0.6953</i> (p=0.0000)	<i>0.4509</i> (p=0.0109)	<i>0.4154</i> (p=0.0201)	(0.05718) (p=0.7600)	0.0753 (p=0.6872)	(0.2005) (p=0.2795)
Trachea	0.167 (p=0.3693)	X	X	(0.3078) (p=0.0920)	X	(0.3451) (p=0.0573)
Caudal Bronchi	<i>0.5488</i> (p=0.0014)	<i>0.3881</i> (p=0.0310)	<i>0.5245</i> (p=0.0025)	0.04305 (p=0.8181)	(0.2555) (p=0.1653)	(0.2218) (p=0.2305)
Heart	0.1158 (p=0.5350)	X	0.1452 (p=0.4358)	(0.08944) (p=0.6323)	X	(0.05976) (p=0.7495)
CdVC	0.1724 (p=0.3537)	<i>0.4475</i> (p=0.0116)	0.130 (p=0.5815)	(0.2022) (p=0.2755)	(0.2094) (p=0.2583)	0.09982 (p=0.5932)
Aorta	0.3518 (p=0.0522)	0.2347 (p=0.2038)	<i>0.3599</i> (p=0.0467)	(0.2012) (p=0.2779)	(0.1071) (p=0.5662)	(0.06351) (p=0.7343)
Spine	<i>0.5421</i> (p=0.0016)	X	X	0.1969 (p=0.2885)	X	(0.2229) (p=0.2281)
Overall	<i>0.6754</i> (p=0.0000)	<i>0.5848</i> (p=0.0006)	<i>0.5292</i> (p=0.022)	(0.1327) (p=0.4768)	(0.2338) (p=0.2056)	(0.2105) (p=0.2557)
<b>Whole-Body</b>	<b>Obs1 : Obs3</b>	<b>Obs1 : Obs2</b>	<b>Obs2 : Obs3</b>	<b>Obs1 : Obs4</b>	<b>Obs2 : Obs4</b>	<b>Obs3 : Obs4</b>
Caudal Pulmonary Vasculature	<i>0.7707</i> (p=0.0000)	<i>0.4969</i> (p=0.0045)	0.3049 (p=0.0954)	(0.2284) (p=0.2166)	X	(0.01539) (p=0.9345)
Trachea	0.2508 (p=0.1735)	X	X	(0.01968) (p=0.9163)	X	<i>(0.5903)</i> (p=0.0005)
Caudal Bronchi	0.1736 (p=0.3504)	0.2208 (p=0.2327)	0.1586 (p=0.3940)	(0.246) (p=0.1823)	(0.1476 ) (p=0.4282)	<i>(0.4431)</i> (p=0.0125)
Heart	0.2473 (p=0.1877)	X	X	(0.07284) (p=0.7021)	X	(0.1077) (p=0.5642)
CdVC	<i>0.5428</i> (p=0.0016)	<i>0.5811</i> (p=0.0006)	<i>0.4313</i> (p=0.0154)	(0.08186) (p=0.6615)	0.01242 (p=0.9471)	(0.09384) (p=0.6156)
Aorta	0.2427 (p=0.1883)	<i>0.5817</i> (p=0.0006)	0.2508 (p=0.1735)	(0.1102) (p=0.5550)	0.02707 (p=0.8851)	(0.239) (p=0.1954)
Spine	0.3263 (p=0.0733)	X	X	(0.2983) (p=0.1031)	X	(0.1222) (p=0.5125)
Overall	<i>0.4201</i> (p=0.0186)	<i>0.5658</i> (p=0.0009)	<i>0.441</i> (p=0.0130)	(0.2078) (p=0.2619)	(0.2468) (p=0.1808)	(0.1466) (p=0.4314)

Table 6 (cont.)

<b>Ventrodorsal</b>				
<b>Collimated</b>	<b>Obs1 : Obs5</b>	<b>Obs2 : Obs5</b>	<b>Obs3 : Obs5</b>	<b>Obs4 : Obs5</b>
Caudal Pulmonary Vasculature	0.4855 ( <i>p</i> =0.0056)	0.575 ( <i>p</i> =0.0007)	0.6096 ( <i>p</i> =0.0003)	(0.2948) ( <i>p</i> =0.1074)
Trachea	0 ( <i>p</i> =1.0000)	(0.3147) ( <i>p</i> =0.0847)	-0.307 ( <i>p</i> =0.0847)	0.2128 ( <i>p</i> =0.2504)
Caudal Bronchi	0.1119 ( <i>p</i> =0.5491)	0.1989 (0.2834)	0.2135 ( <i>p</i> =0.2488)	(0.314) ( <i>p</i> =0.0854)
Heart	X	X	X	X
CdVC	0.7462 ( <i>P</i> <0.0001)	0.2208 ( <i>p</i> =0.2237)	0.4962 ( <i>p</i> =0.0045)	(0.1854) ( <i>p</i> =0.3181)
Aorta	0.5482 ( <i>p</i> =0.0014)	0.4244 ( <i>p</i> =0.0173)	0.3057 ( <i>p</i> =0.0945)	0.05631 ( <i>p</i> =0.7635)
Spine	0.2831 ( <i>p</i> =0.1227)	0.2565 ( <i>p</i> =0.1637)	X	(0.04795) ( <i>p</i> =0.7978)
Overall	0.7108 ( <i>p</i> <0.0001)	0.5664 ( <i>p</i> =0.0009)	0.6853 ( <i>p</i> <0.0001)	(0.1822) ( <i>p</i> =0.3267)
<b>Whole-Body</b>	<b>Obs1 : Obs3</b>	<b>Obs1 : Obs2</b>	<b>Obs2 : Obs3</b>	<b>Obs1 : Obs4</b>
Caudal Pulmonary Vasculature	0.3402 ( <i>p</i> =0.0612)	0.2503 ( <i>p</i> =0.1745)	0.4875 ( <i>p</i> =0.0054)	(0.07737) ( <i>p</i> =0.6791)
Trachea	0.2112 ( <i>p</i> =0.2540)	0.2215 ( <i>p</i> =0.2315)	X	(0.1605) ( <i>p</i> =0.3883)
Caudal Bronchi	0.229 ( <i>p</i> =0.2153)	0.0508 ( <i>p</i> =0.7861)	0.4163 ( <i>p</i> =0.0198)	(0.2236) ( <i>p</i> =0.2265)
Heart	0.523 ( <i>p</i> =0.0030)	0.3057 ( <i>p</i> =0.0945)	X	(0.05976) ( <i>p</i> =0.7495)
CdVC	0.7127 ( <i>p</i> <0.0001)	0.5605 ( <i>p</i> =0.0010)	0.5766 ( <i>p</i> =0.0007)	(0.2186) ( <i>p</i> =0.2374)
Aorta	0.5663 ( <i>p</i> =0.0009)	0.3961 ( <i>p</i> =0.0274)	0.4067 ( <i>p</i> =0.0232)	0.004258 ( <i>p</i> =0.9784)
Spine	0.6124 ( <i>p</i> =0.0003)	0.4897 ( <i>p</i> =0.0052)	X	(0.04259) ( <i>p</i> =0.8200)
Overall	0.5936 ( <i>p</i> =0.0004)	0.4714 ( <i>p</i> =0.0074)	0.5703 ( <i>p</i> =0.0008)	(0.2306) ( <i>p</i> =0.2121)



The overall counts and frequencies for each grade and each observer for each rating category are listed in **Table 7**. In all of the observers, only three images, all from the whole-body ventrodorsal group, were given an overall quality rating of 1. There were also only 44 grades of 2 out of 620 total overall quality ratings (7.1%). Therefore only 47 out of 620 ratings (7.58%) were considered to be below adequate in image quality by the observers. The vast majority of images, whether obtained using collimated or whole-body technique, were graded as at least adequate in quality by the observers.

**Table 7. Counts (and frequencies) for each grade for each observer for the lateral images.**

Grade	Observer 1		Observer 2		Observer 3		Observer 4		Observer 5	
	Collimated	Whole-Body	Collimated	Whole-Body	Collimated	Whole-Body	Collimated	Whole-Body	Collimated	Whole-Body
<b>Lateral Overall</b>										
1	0 (0%)	0 (0%)	0 (0%)	0 (0%)	0 (0%)	0 (0%)	0 (0%)	0 (0%)	0 (0%)	0 (0%)
2	1 (3.2%)	2 (6.5%)	0 (0%)	0 (0%)	1 (3.2%)	1 (3.2%)	0 (0%)	0 (0%)	2 (6.5%)	6 (19.4%)
3	15 (48.4%)	19 (61.3%)	1 (3.2%)	0 (0%)	6 (22.6%)	11 (35.5%)	2 (6.5%)	7 (22.6%)	8 (25.8%)	5 (16.1%)
4	13 (41.9%)	10 (32.3%)	10 (32.3%)	10 (32.3%)	13 (38.7%)	14 (45.2%)	17 (54.8%)	18 (58.1%)	11 (35.5%)	13 (41.9%)
5	2 (6.5%)	0 (0%)	20 (64.5%)	21 (67.7%)	11 (35.5%)	5 (16.1%)	12 (38.7%)	6 (19.4%)	10 (32.3%)	7 (22.6%)

Grade	Observer 1		Observer 2		Observer 3		Observer 4		Observer 5	
	Collimated	Whole-Body	Collimated	Whole-Body	Collimated	Whole-Body	Collimated	Whole-Body	Collimated	Whole-Body
<b>Pulmonary Vasculature</b>										
1	2 (6.5%)	3 (9.7%)	2 (6.5%)	0 (0%)	4 (12.9%)	6 (19.4%)	2 (6.5%)	3 (9.7%)	2 (6.5%)	3 (9.7%)
2	11 (35.5%)	13 (41.9%)	11 (35.5%)	11 (35.5%)	14 (45.2%)	13 (41.9%)	7 (22.6%)	11 (35.5%)	15 (48.4%)	15 (48.4%)
3	18 (58.1%)	15 (48.4%)	18 (58.1%)	20 (64.5%)	13 (41.9%)	12 (38.7%)	22 (71%)	17 (54.8%)	14 (45.2%)	13 (41.9%)
<b>Pulmonary Vasculature</b>										
1	9 (29.0%)	11 (35.5%)	1 (3.2%)	0 (0%)	0 (0%)	0 (0%)	0 (0%)	0 (0%)	10 (32.3%)	9 (29%)
2	8 (25.8%)	16 (51.6%)	7 (22.6%)	12 (38.7%)	8 (25.8%)	10 (32.3%)	9 (29%)	13 (41.9%)	21 (67.7%)	22 (71%)
3	14 (45.2%)	4 (12.9%)	23 (74.2%)	19 (61.3%)	23 (74.2%)	21 (67.7%)	22 (71%)	18 (58.1%)	0 (0%)	0 (0%)
<b>Trachea</b>										
1	0 (0%)	0 (0%)	0 (0%)	0 (0%)	0 (0%)	1 (3.2%)	0 (0%)	0 (0%)	0 (0%)	0 (0%)
2	8 (25.8%)	12 (38.7%)	0 (0%)	0 (0%)	14 (45.2%)	18 (58.1%)	4 (12.9%)	13 (41.9%)	0 (0%)	3 (9.7%)
3	23 (74.2%)	19 (61.3%)	31 (100%)	31 (100%)	17 (54.8%)	12 (38.7%)	27 (87.1%)	18 (58.1%)	31 (100%)	28 (90.3%)
<b>Caudal Bronchi</b>										
1	0 (0%)	2 (6.5%)	0 (0%)	0 (0%)	0 (0%)	0 (0%)	0 (0%)	0 (0%)	0 (0%)	1 (3.2%)
2	20 (64.5%)	20 (64.5%)	1 (3.2%)	1 (3.2%)	5 (16.1%)	8 (25.8%)	11 (35.5%)	14 (45.2%)	31 (100%)	30 (96.8%)
3	11 (35.5%)	9 (29.0%)	30 (96.8%)	30 (96.8%)	26 (83.9%)	23 (74.2%)	20 (64.5%)	17 (54.8%)	0 (0%)	0 (0%)
<b>Heart</b>										
1	2 (6.5%)	6 (19.4%)	0 (0%)	0 (0%)	0 (0%)	0 (0%)	0 (0%)	0 (0%)	0 (0%)	0 (0%)
2	17 (54.8%)	17 (54.8%)	2 (6.5%)	2 (6.5%)	4 (12.9%)	9 (29%)	6 (19.4%)	15 (48.4%)	4 (12.9%)	6 (19.4%)
3	12 (38.7%)	8 (25.8%)	29 (93.5%)	29 (93.5%)	27 (87.1%)	22 (71%)	25 (80.6%)	16 (51.6%)	27 (87.1%)	25 (90.6%)
<b>Ribs</b>										
1	1 (3.2%)	2 (6.5%)	0 (0%)	0 (0%)	0 (0%)	0 (0%)	0 (0%)	0 (0%)	0 (0%)	0 (0%)
2	17 (54.8%)	19 (61.3%)	0 (0%)	0 (0%)	10 (32.3%)	16 (51.6%)	6 (19.4%)	18 (58.1%)	3 (9.7%)	4 (12.9%)
3	13 (41.9%)	10 (32.3%)	31 (100%)	31 (100%)	21 (67.7%)	15 (48.4%)	25 (80.6%)	13 (41.9%)	28 (90.3%)	27 (87.1%)

**Table 8. Counts (and frequencies) for each grade for each observer for the ventrodorsal images.**

Grade	Observer 1		Observer 2		Observer 3		Observer 4		Observer 5	
	Collimated	Whole-Body	Collimated	Whole-Body	Collimated	Whole-Body	Collimated	Whole-Body	Collimated	Whole-Body
<b>VD Overall</b>										
1	0 (0%)	0 (0%)	0 (0%)	0 (0%)	0 (0%)	2 (6.5%)	0 (0%)	0 (0%)	0 (0%)	1 (3.2%)
2	2 (6.5%)	6 (19.4%)	0 (0%)	0 (0%)	6 (19.4%)	13 (41.9%)	0 (0%)	0 (0%)	1 (3.2%)	3 (9.7%)
3	9 (29.0%)	16 (51.6%)	0 (0%)	1 (3.2%)	4 (12.9%)	7 (22.6%)	1 (3.2%)	9 (29%)	6 (19.4%)	13 (41.9%)
4	18 (58.1%)	8 (25.8%)	9 (29%)	19 (61.3%)	12 (38.7%)	6 (19.4%)	21 (67.7%)	18 (58.1%)	8 (25.8%)	12 (38.7%)
5	2 (6.5%)	1 (3.2%)	22 (71%)	11 (35.5%)	9 (29%)	3 (9.7%)	9 (29.0%)	4 (12.9%)	16 (51.6%)	2 (6.5%)

Grade	Observer 1		Observer 2		Observer 3		Observer 4		Observer 5	
	Collimated	Whole-Body	Collimated	Whole-Body	Collimated	Whole-Body	Collimated	Whole-Body	Collimated	Whole-Body
<b>Cd Pulmonary Vasculature</b>										
1	3 (9.7%)	9 (29.0%)	0 (0%)	0 (0%)	4 (12.9%)	9 (29%)	0 (0%)	1 (3.2%)	0 (0%)	6 (19.4%)
2	14 (45.2%)	16 (51.6%)	12 (38.7%)	18 (58.1%)	9 (29%)	15 (48.4%)	9 (29%)	19 (61.3%)	14 (45.2%)	23 (74.2%)
3	14 (45.2%)	6 (19.4%)	19 (61.3%)	13 (41.9%)	18 (58.1%)	7 (22.6%)	22 (71%)	11 (35.5%)	17 (54.8%)	2 (6.5%)
<b>Trachea</b>										
1	8 (25.8%)	13 (41.9%)	0 (0%)	0 (0%)	2 (6.5%)	8 (25.8%)	0 (0%)	0 (0%)	4 (12.9%)	5 (16.1%)
2	15 (48.4%)	12 (38.7%)	0 (0%)	0 (0%)	18 (58.1%)	18 (58.1%)	8 (25.8%)	18 (58.1%)	27 (87.1%)	26 (83.9%)
3	8 (25.8%)	6 (19.4%)	31 (100%)	31 (100%)	11 (35.5%)	5 (16.1%)	23 (74.2%)	13 (41.9%)	0 (0%)	0 (0%)
<b>Caudal Bronchi</b>										
1	9 (29.0%)	15 (48.4%)	0 (0%)	0 (0%)	3 (9.7%)	9 (29%)	0 (0%)	0 (0%)	3 (9.7%)	13 (41.9%)
2	15 (48.4%)	12 (38.7%)	13 (41.9%)	25 (80.6%)	18 (58.1%)	19 (61.3%)	9 (29%)	16 (51.6%)	27 (87.1%)	18 (58.1%)
3	7 (22.6%)	4 (12.9%)	18 (58.1%)	6 (19.4%)	10 (32.3%)	3 (9.7%)	22 (71%)	15 (48.4%)	1 (3.2%)	0 (0%)
<b>Heart</b>										
1	0 (0%)	0 (0%)	0 (0%)	0 (0%)	0 (0%)	0 (0%)	0 (0%)	0 (0%)	0 (0%)	0 (0%)
2	6 (19.4%)	4 (13.3%)	0 (0%)	0 (0%)	3 (9.7%)	8 (25.8%)	1 (3.2%)	1 (3.2%)	0 (0%)	2 (9.7%)
3	25 (80.6%)	26 (86.7%)	31 (100%)	31 (100%)	28 (90.3%)	23 (74.2%)	30 (96.8%)	30 (96.8%)	31 (100%)	28 (90.3%)
<b>CdCV</b>										
1	3 (9.7%)	6 (19.4%)	0 (0%)	0 (0%)	1 (3.2%)	7 (22.6%)	0 (0%)	0 (0%)	1 (3.2%)	2 (6.5%)
2	8 (25.8%)	11 (35.5%)	3 (9.7%)	4 (12.9%)	10 (32.3%)	15 (48.4%)	9 (29%)	15 (48.4%)	10 (32.3%)	10 (32.3%)
3	20 (64.5%)	14 (45.2%)	28 (90.3%)	27 (87.1%)	20 (64.5%)	9 (29%)	22 (71%)	16 (51.6%)	20 (64.5%)	19 (61.3%)
<b>Aorta</b>										
1	4 (12.9%)	12 (38.7%)	0 (0%)	0 (0%)	1 (3.2%)	2 (6.5%)	0 (0%)	0 (0%)	0 (0%)	0 (0%)
2	15 (48.4%)	13 (41.9%)	3 (9.7%)	10 (32.3%)	12 (38.7%)	20 (64.5%)	3 (9.7%)	18 (58.1%)	8 (25.8%)	19 (61.3%)
3	12 (38.7%)	6 (19.4%)	28 (90.3%)	21 (67.7%)	18 (58.1%)	9 (29%)	28 (90.3%)	13 (41.9%)	23 (74.2%)	12 (38.7%)
<b>Spine</b>										
1	13 (41.9%)	17 (54.8%)	0 (0%)	0 (0%)	5 (16.1%)	9 (29%)	0 (0%)	0 (0%)	0 (0%)	0 (0%)
2	11 (35.6%)	12 (38.7%)	0 (0%)	0 (0%)	15 (48.4%)	18 (58.1%)	1 (3.2%)	7 (22.6%)	2 (6.5%)	10 (32.3%)
3	7 (22.6%)	2 (6.5%)	31 (100%)	31 (100%)	11 (35.5%)	4 (12.9%)	30 (96.8%)	24 (77.4%)	29 (93.5%)	21 (67.7%)

The grades for the collimated and whole-body approaches for each observer in each criterion were compared using the Wilcoxon signed-rank test (**Table 9**). Observer 1 had significantly higher grades for collimated images for the caudal pulmonary vasculature on the lateral and ventrodorsal images, for the aorta on the ventrodorsal images, and in the overall grade for the ventrodorsal images. The difference neared significance for the heart and the overall ratings on the lateral images and for the caudal bronchi on the ventrodorsal images. Observer 2 had significantly higher ratings for collimated images for the caudal bronchi and aorta on the ventrodorsal images, as well as for the overall grade for the ventrodorsal images. Observer 3 had significantly higher ratings for collimated images for the caudal pulmonary vasculature, the trachea, the caudal bronchi, the caudal vena cava, and the caudal spine on the ventrodorsal images, as well as for the overall grade for the ventrodorsal images. The difference neared significance for the overall grades for the lateral images. Observer 4 had significantly higher ratings for collimated images for the trachea, heart, ribs, and overall rating on the lateral images, and for the caudal pulmonary vasculature, the trachea, the aorta and the overall grade on the ventrodorsal images. The difference neared significance for the caudal bronchi and spine on the ventrodorsal images. Mean grades were also calculated for each observer for each rating category (**Table 10**). This was done to provide a quick comparison of the distributions of grades for each approach, even though the validity of calculating and comparing means for ordinal data is questionable. For almost all observers and all categories, the mean grade of the collimated images was higher than the mean grade of the whole-body images. Histograms of the distributions of grades for each observer for overall image quality were created (**Figs. 3-4**).

Table 9. p values calculated from Wilcoxon signed-rank comparison of the grades for the collimated and whole body approach for each observer. Categories with significant results are italicized (P < 0.05 was considered significant. An X indicates too few differences in rank between groups for a p value to be calculated).

<b>LATERAL</b>	Observer 1	Observer 2	Observer 3	Observer 4	Observer 4
<b>Cranial Pulmonary Vasculature</b>	0.4212	0.3757	0.5798	0.2943	0.6698
<b>Caudal Pulmonary Vasculature</b>	<i>0.0267</i>	0.5245	0.5469	0.3394	0.8311
<b>Trachea</b>	0.25	0.25	0.1475	<i>0.0137</i>	X
<b>Caudal Bronchi</b>	0.3575	X	0.3125	0.4648	0.0674
<b>Heart</b>	0.0771	X	0.2439	<i>0.0266</i>	X
<b>Ribs</b>	0.2754	X	0.1294	<i>0.0023</i>	0.8125
<b>Overall</b>	0.0946	0.6221	0.0885	<i>0.0214</i>	0.1928
<b>VENTRODORSAL</b>					
<b>Caudal Pulmonary Vasculature</b>	<i>0.0139</i>	0.1055	<i>0.0021</i>	<i>0.0129</i>	<i>&lt;0.0001</i>
<b>Trachea</b>	0.1901	X	<i>0.0172</i>	<i>0.025</i>	0.8203
<b>Caudal Bronchi</b>	0.0654	<i>0.0023</i>	<i>0.0155</i>	0.0942	<i>0.0103</i>
<b>Heart</b>	0.5469	X	0.1641	X	<i>0.0539</i>
<b>CdVC</b>	0.1415	0.8125	<i>0.0017</i>	0.1928	0.6788
<b>Aorta</b>	<i>0.0172</i>	<i>0.0391</i>	0.0448	<i>0.0014</i>	<i>&lt;0.0001</i>
<b>Spine</b>	0.108	X	<i>0.0256</i>	0.0547	<i>0.0078</i>
<b>Overall</b>	<i>0.0136</i>	<i>0.0023</i>	<i>0.0013</i>	<i>0.0182</i>	<i>0.0007</i>

Table 10. Mean grade for each observer for each criteria for each image type.

<b>LATERAL</b>	Observer 1		Observer 2		Observer 3		Observer 4		Observer 5	
	Collimated	Whole-Body	Collimated	Whole-Body	Collimated	Whole-Body	Collimated	Whole-Body	Collimated	Whole-Body
<b>Cranial Pulmonary</b>	2.5161	2.3871	2.5161	2.6452	2.2903	2.1935	2.6452	2.4516	2.387	2.323
<b>Caudal Pulmonary</b>	2.1613	1.7742	2.7097	2.6129	2.7419	2.6774	2.7097	2.5806	1.677	1.71
<b>Trachea</b>	2.7419	2.6129	3	3	2.5484	2.3548	2.871	2.5806	3	2.903
<b>Caudal Bronchi</b>	2.3548	2.2258	2.9677	2.9677	2.8387	2.7419	2.6452	2.5484	2	1.968
<b>Heart</b>	2.3226	2.0645	2.9355	2.9355	2.871	2.7097	2.8065	2.5161	2.871	2.806
<b>Ribs</b>	2.3871	2.2581	3	3	2.6774	2.4839	2.8065	2.4194	2.903	2.871
<b>Overall</b>	3.5161	3.2581	4.6129	4.6774	4.0968	3.7419	4.3226	3.9677	3.935	3.677
<b>VENTRODORSAL</b>										
<b>Caudal Pulmonary</b>	2.3548	1.9032	2.6129	2.4194	2.4516	1.9355	2.7097	2.3226	2.548	1.871
<b>Trachea</b>	2	1.7742	2	2	2.2903	1.9032	2.7419	2.4194	1.871	1.839
<b>Caudal Bronchi</b>	1.9355	1.6452	2.5806	2.1935	2.2258	1.8065	2.7097	2.4839	1.935	1.581
<b>Heart</b>	2.8065	2.867	3	3	2.9032	2.7419	2.7419	2.9677	3	2.903
<b>CdVC</b>	2.5484	2.2581	2.9032	2.871	2.6129	2.0645	2.7097	2.5161	2.613	2.548
<b>Aorta</b>	2.2581	1.8065	2.9302	2.6774	2.5484	2.2258	2.9032	2.4194	2.742	2.387
<b>Spine</b>	1.8065	1.5161	3	3	2.1935	1.8387	2.9677	2.7742	2.935	2.677
<b>Overall</b>	3.6452	3.129	4.7097	4.3226	3.7742	2.8387	4.2581	3.8387	4.258	3.355

**Table 11. Histograms of overall image quality grades for each observer for the lateral images**

	Collimated	Whole-Body																				
Obs1	<table border="1"> <caption>Data for Obs1 Collimated</caption> <thead> <tr><th>Grade</th><th>Frequency</th></tr> </thead> <tbody> <tr><td>2</td><td>1</td></tr> <tr><td>3</td><td>15</td></tr> <tr><td>4</td><td>13</td></tr> <tr><td>6</td><td>2</td></tr> </tbody> </table>	Grade	Frequency	2	1	3	15	4	13	6	2	<table border="1"> <caption>Data for Obs1 Whole-Body</caption> <thead> <tr><th>Grades</th><th>Frequency</th></tr> </thead> <tbody> <tr><td>2</td><td>2</td></tr> <tr><td>3</td><td>19</td></tr> <tr><td>4</td><td>10</td></tr> </tbody> </table>	Grades	Frequency	2	2	3	19	4	10		
Grade	Frequency																					
2	1																					
3	15																					
4	13																					
6	2																					
Grades	Frequency																					
2	2																					
3	19																					
4	10																					
Obs2	<table border="1"> <caption>Data for Obs2 Collimated</caption> <thead> <tr><th>Grade</th><th>Frequency</th></tr> </thead> <tbody> <tr><td>3</td><td>1</td></tr> <tr><td>4</td><td>10</td></tr> <tr><td>6</td><td>20</td></tr> </tbody> </table>	Grade	Frequency	3	1	4	10	6	20	<table border="1"> <caption>Data for Obs2 Whole-Body</caption> <thead> <tr><th>Grade</th><th>Frequency</th></tr> </thead> <tbody> <tr><td>4</td><td>10</td></tr> <tr><td>6</td><td>21</td></tr> </tbody> </table>	Grade	Frequency	4	10	6	21						
Grade	Frequency																					
3	1																					
4	10																					
6	20																					
Grade	Frequency																					
4	10																					
6	21																					
Obs3	<table border="1"> <caption>Data for Obs3 Collimated</caption> <thead> <tr><th>Grade</th><th>Frequency</th></tr> </thead> <tbody> <tr><td>2</td><td>1</td></tr> <tr><td>3</td><td>6</td></tr> <tr><td>4</td><td>13</td></tr> <tr><td>5</td><td>11</td></tr> </tbody> </table>	Grade	Frequency	2	1	3	6	4	13	5	11	<table border="1"> <caption>Data for Obs3 Whole-Body</caption> <thead> <tr><th>Grade</th><th>Frequency</th></tr> </thead> <tbody> <tr><td>2</td><td>1</td></tr> <tr><td>3</td><td>11</td></tr> <tr><td>4</td><td>14</td></tr> <tr><td>6</td><td>5</td></tr> </tbody> </table>	Grade	Frequency	2	1	3	11	4	14	6	5
Grade	Frequency																					
2	1																					
3	6																					
4	13																					
5	11																					
Grade	Frequency																					
2	1																					
3	11																					
4	14																					
6	5																					
Obs4	<table border="1"> <caption>Data for Obs4 Collimated</caption> <thead> <tr><th>Grade</th><th>Frequency</th></tr> </thead> <tbody> <tr><td>3</td><td>2</td></tr> <tr><td>4</td><td>17</td></tr> <tr><td>5</td><td>12</td></tr> </tbody> </table>	Grade	Frequency	3	2	4	17	5	12	<table border="1"> <caption>Data for Obs4 Whole-Body</caption> <thead> <tr><th>Grade</th><th>Frequency</th></tr> </thead> <tbody> <tr><td>3</td><td>7</td></tr> <tr><td>4</td><td>18</td></tr> <tr><td>6</td><td>6</td></tr> </tbody> </table>	Grade	Frequency	3	7	4	18	6	6				
Grade	Frequency																					
3	2																					
4	17																					
5	12																					
Grade	Frequency																					
3	7																					
4	18																					
6	6																					
Obs5	<table border="1"> <caption>Data for Obs5 Collimated</caption> <thead> <tr><th>Grade</th><th>Frequency</th></tr> </thead> <tbody> <tr><td>2</td><td>2</td></tr> <tr><td>3</td><td>8</td></tr> <tr><td>4</td><td>11</td></tr> <tr><td>5</td><td>10</td></tr> </tbody> </table>	Grade	Frequency	2	2	3	8	4	11	5	10	<table border="1"> <caption>Data for Obs5 Whole-Body</caption> <thead> <tr><th>Grade</th><th>Frequency</th></tr> </thead> <tbody> <tr><td>2</td><td>6</td></tr> <tr><td>3</td><td>5</td></tr> <tr><td>4</td><td>13</td></tr> <tr><td>6</td><td>7</td></tr> </tbody> </table>	Grade	Frequency	2	6	3	5	4	13	6	7
Grade	Frequency																					
2	2																					
3	8																					
4	11																					
5	10																					
Grade	Frequency																					
2	6																					
3	5																					
4	13																					
6	7																					

**Table 12. Histograms of overall image quality grades for each observer for the ventrodorsal images**

	Collimated	Whole-Body																						
Obs1	<table border="1"> <caption>Data for Obs1 Collimated</caption> <thead> <tr><th>Grade</th><th>Frequency</th></tr> </thead> <tbody> <tr><td>2</td><td>2</td></tr> <tr><td>3</td><td>9</td></tr> <tr><td>4</td><td>18</td></tr> <tr><td>5</td><td>2</td></tr> </tbody> </table>	Grade	Frequency	2	2	3	9	4	18	5	2	<table border="1"> <caption>Data for Obs1 Whole-Body</caption> <thead> <tr><th>Grade</th><th>Frequency</th></tr> </thead> <tbody> <tr><td>2</td><td>6</td></tr> <tr><td>3</td><td>16</td></tr> <tr><td>4</td><td>8</td></tr> <tr><td>5</td><td>1</td></tr> </tbody> </table>	Grade	Frequency	2	6	3	16	4	8	5	1		
Grade	Frequency																							
2	2																							
3	9																							
4	18																							
5	2																							
Grade	Frequency																							
2	6																							
3	16																							
4	8																							
5	1																							
Obs2	<table border="1"> <caption>Data for Obs2 Collimated</caption> <thead> <tr><th>Grade</th><th>Frequency</th></tr> </thead> <tbody> <tr><td>4</td><td>9</td></tr> <tr><td>5</td><td>34</td></tr> </tbody> </table>	Grade	Frequency	4	9	5	34	<table border="1"> <caption>Data for Obs2 Whole-Body</caption> <thead> <tr><th>Grade</th><th>Frequency</th></tr> </thead> <tbody> <tr><td>3</td><td>1</td></tr> <tr><td>4</td><td>19</td></tr> <tr><td>5</td><td>11</td></tr> </tbody> </table>	Grade	Frequency	3	1	4	19	5	11								
Grade	Frequency																							
4	9																							
5	34																							
Grade	Frequency																							
3	1																							
4	19																							
5	11																							
Obs3	<table border="1"> <caption>Data for Obs3 Collimated</caption> <thead> <tr><th>Grade</th><th>Frequency</th></tr> </thead> <tbody> <tr><td>2</td><td>6</td></tr> <tr><td>3</td><td>4</td></tr> <tr><td>4</td><td>12</td></tr> <tr><td>5</td><td>8</td></tr> </tbody> </table>	Grade	Frequency	2	6	3	4	4	12	5	8	<table border="1"> <caption>Data for Obs3 Whole-Body</caption> <thead> <tr><th>Grade</th><th>Frequency</th></tr> </thead> <tbody> <tr><td>1</td><td>2</td></tr> <tr><td>2</td><td>13</td></tr> <tr><td>3</td><td>7</td></tr> <tr><td>4</td><td>6</td></tr> <tr><td>5</td><td>3</td></tr> </tbody> </table>	Grade	Frequency	1	2	2	13	3	7	4	6	5	3
Grade	Frequency																							
2	6																							
3	4																							
4	12																							
5	8																							
Grade	Frequency																							
1	2																							
2	13																							
3	7																							
4	6																							
5	3																							
Obs4	<table border="1"> <caption>Data for Obs4 Collimated</caption> <thead> <tr><th>Grade</th><th>Frequency</th></tr> </thead> <tbody> <tr><td>3</td><td>1</td></tr> <tr><td>4</td><td>21</td></tr> <tr><td>5</td><td>9</td></tr> </tbody> </table>	Grade	Frequency	3	1	4	21	5	9	<table border="1"> <caption>Data for Obs4 Whole-Body</caption> <thead> <tr><th>Grade</th><th>Frequency</th></tr> </thead> <tbody> <tr><td>1</td><td>1</td></tr> <tr><td>2</td><td>3</td></tr> <tr><td>3</td><td>13</td></tr> <tr><td>4</td><td>12</td></tr> <tr><td>5</td><td>2</td></tr> </tbody> </table>	Grade	Frequency	1	1	2	3	3	13	4	12	5	2		
Grade	Frequency																							
3	1																							
4	21																							
5	9																							
Grade	Frequency																							
1	1																							
2	3																							
3	13																							
4	12																							
5	2																							
Obs5	<table border="1"> <caption>Data for Obs5 Collimated</caption> <thead> <tr><th>Grade</th><th>Frequency</th></tr> </thead> <tbody> <tr><td>2</td><td>1</td></tr> <tr><td>3</td><td>6</td></tr> <tr><td>4</td><td>9</td></tr> <tr><td>5</td><td>16</td></tr> </tbody> </table>	Grade	Frequency	2	1	3	6	4	9	5	16	<table border="1"> <caption>Data for Obs5 Whole-Body</caption> <thead> <tr><th>Grade</th><th>Frequency</th></tr> </thead> <tbody> <tr><td>1</td><td>1</td></tr> <tr><td>2</td><td>3</td></tr> <tr><td>3</td><td>13</td></tr> <tr><td>4</td><td>12</td></tr> <tr><td>5</td><td>2</td></tr> </tbody> </table>	Grade	Frequency	1	1	2	3	3	13	4	12	5	2
Grade	Frequency																							
2	1																							
3	6																							
4	9																							
5	16																							
Grade	Frequency																							
1	1																							
2	3																							
3	13																							
4	12																							
5	2																							

The  $AUC_{VGC}$  was determined for each observer for each criterion (**Table 13**). For all categories and all observers, the  $AUC_{VGC}$  was 0.5 or higher. Based on the way the two approaches were plotted in this study, this indicates that all observers found higher image quality for the collimated approach compared to the whole-body approach or no difference between the approaches. For no observer and no criteria was the whole-body projection found to be superior to the collimated projection. For almost all categories the  $AUC_{VGC}$  was actually greater than 0.5, indicating superior quality of the collimated projections compared to the whole-body. However, for most sets of observations the 95% confidence interval for the  $AUC_{VGC}$  included 0.5, indicating that the difference in perceived image quality between the imaging approaches was not statistically significant. A statistically significant  $AUC_{VGC}$  was found on 24 of the 75 comparisons (32%). For all four observers, the  $AUC_{VGC}$  for the overall grade of the ventrodorsal projection was significantly greater than 0.5 (**Fig. 3**). Though in general the ratings followed the same trends for all observers across each category, this was the only rating on which all four observers had an  $AUC_{VGC}$  that was significantly greater than 0.5. See appendix 1 for figures showing all VGC curves.



Table 13. The  $AUC_{VGC}$  (and 95% confidence interval) for each observer for each criteria. Curves that significantly differed from 0.5 are italicized.

LATERAL	Observer 1	Observer 2	Observer 3	Observer 4	Observer5
Cranial Pulmonary Vasculature	0.552 (0.420-0.679)	0.544 (0.412-0.671)	0.533 (0.402-0.661)	0.580 (0.448-0.704)	0.524 (0.393-0.653)
Caudal Pulmonary Vasculature	0.632 (0.500-0.751)	0.558 (0.426-0.684)	0.532 (0.401-0.660)	0.565 (0.433-0.690)	0.516 (0.386-0.645)
Trachea	0.565 (0.433-0.690)	0.500 (0.370-0.630)	0.588 (0.456-0.711)	<i>0.645 (0.513-0.763)</i>	0.548 (0.417-0.675)
Caudal Bronchi	0.553 (0.421-0.680)	0.500 (0.370-0.630)	0.548 (0.417-0.675)	0.548 (0.417-0.675)	0.516 (0.386-0.645)
Heart	0.600 (0.468-0.722)	0.500 (0.370-0.630)	0.581 (0.448-0.705)	<i>0.645 (0.513-0.763)</i>	0.532 (0.401-0.660)
Ribs	0.556 (0.424-0.682)	0.500 (0.370-0.630)	0.597 (0.464-0.719)	<i>0.694 (0.563-0.804)</i>	0.516 (0.386-0.645)
Overall	0.597 (0.464-0.719)	0.521 (0.391-0.650)	0.624 (0.492-0.744)	<i>0.640 (0.508-0.758)</i>	0.563 (0.432-0.689)
<b>VENTRODORSAL</b>					
Caudal Pulmonary Vasculature	<i>0.670 (0.539-0.784)</i>	0.597 (0.464-0.719)	<i>0.688 (0.558-0.800)</i>	<i>0.682 (0.552-0.795)</i>	<i>0.786 (0.663-0.880)</i>
Trachea	0.584 (0.452-0.708)	0.500 (0.370-0.630)	<i>0.653 (0.521-0.769)</i>	<i>0.661 (0.530-0.777)</i>	0.516 (0.386-0.645)
Caudal Bronchi	0.609 (0.477-0.731)	<i>0.694 (0.563-0.804)</i>	<i>0.668 (0.536-0.782)</i>	0.613 (0.481-0.734)	<i>0.671 (0.540-0.785)</i>
Heart	0.530 (0.398-0.659)	0.500 (0.369-0.631)	0.568 (0.435-0.695)	0.5 (0.370-0.630)	0.550 (0.417-0.678)
CdVC	0.605 (0.472-0.727)	0.516 (0.386-0.645)	<i>0.706 (0.577-0.815)</i>	0.597 (0.464-0.719)	0.521 (0.391-0.650)
Aorta	<i>0.663 (0.532-0.778)</i>	0.613 (0.481-0.734)	<i>0.647 (0.515-0.764)</i>	0.742 (0.615-0.845)	<i>0.677 (0.547-0.791)</i>
Spine	0.597 (0.464-0.719)	0.500 (0.370-0.630)	<i>0.636 (0.504-0.755)</i>	0.597 (0.464-0.719)	0.629 (0.497-0.748)
Overall	<i>0.688 (0.557-0.800)</i>	<i>0.682 (0.552-0.795)</i>	<i>0.719 (0.590-0.825)</i>	<i>0.670 (0.539-0.784)</i>	<i>0.759 (0.634-0.859)</i>

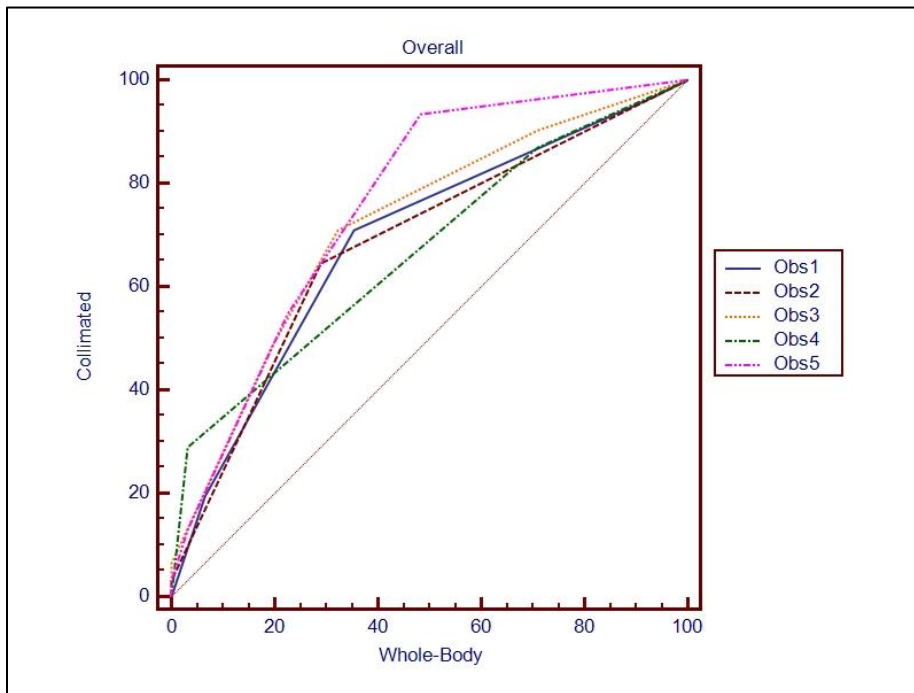


Figure 3. VGC curve comparing overall ratings for images obtained with collimated approach compared to the whole-body approach. All four observers had an  $AUC_{VGC}$  significantly greater than 0.5, indicating significantly higher grades for overall quality in the collimated images.

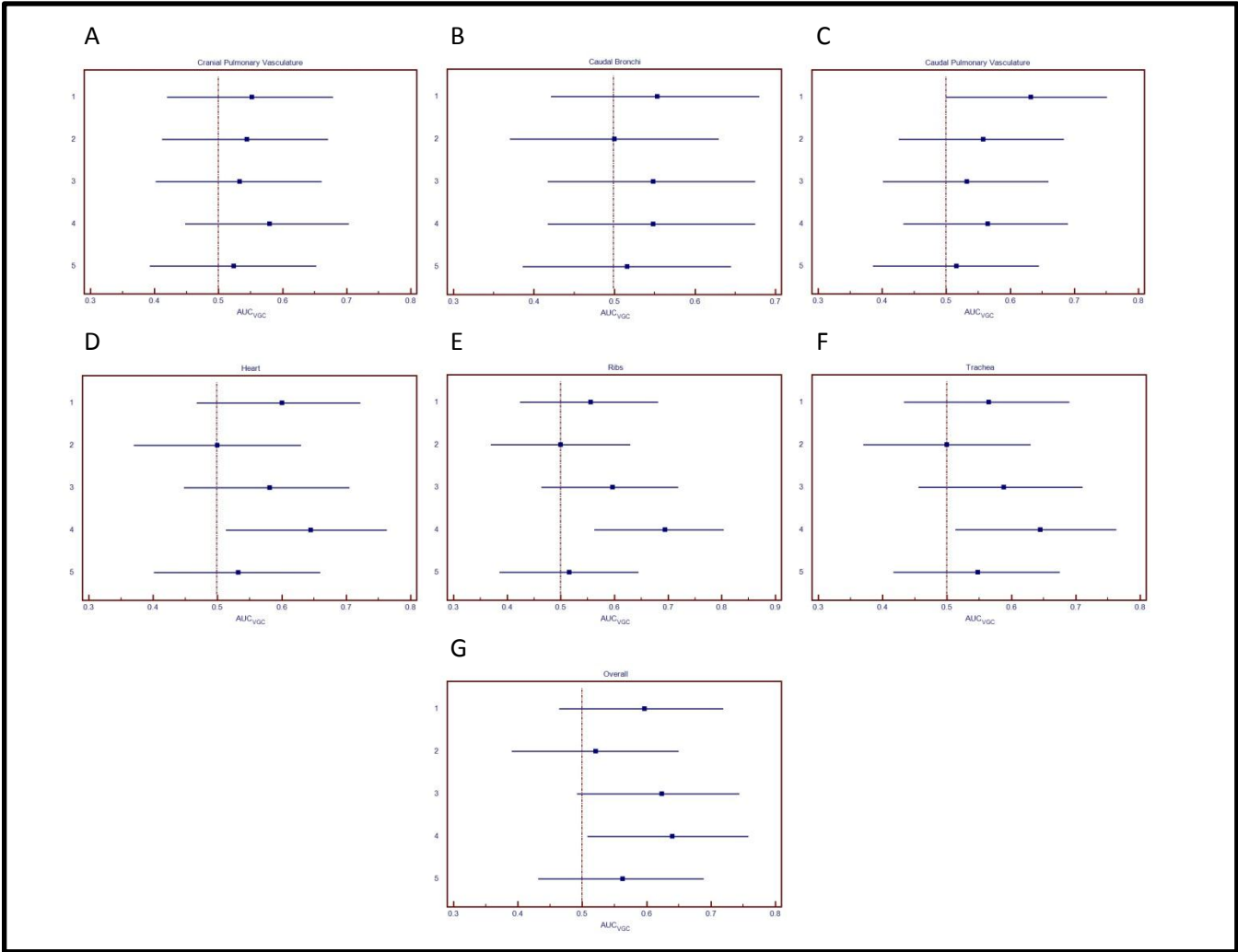


Figure 5. Forest plots of AUCVGC and 95% confidence interval for all observers for the (A) cranial pulmonary vasculature, (B) caudal bronchi, (C) caudal pulmonary vasculature, (D) trachea, (E) heart, (F) ribs, and (G) overall image quality for the lateral images. A vertical line is present at an AUC of 0.5 for reference

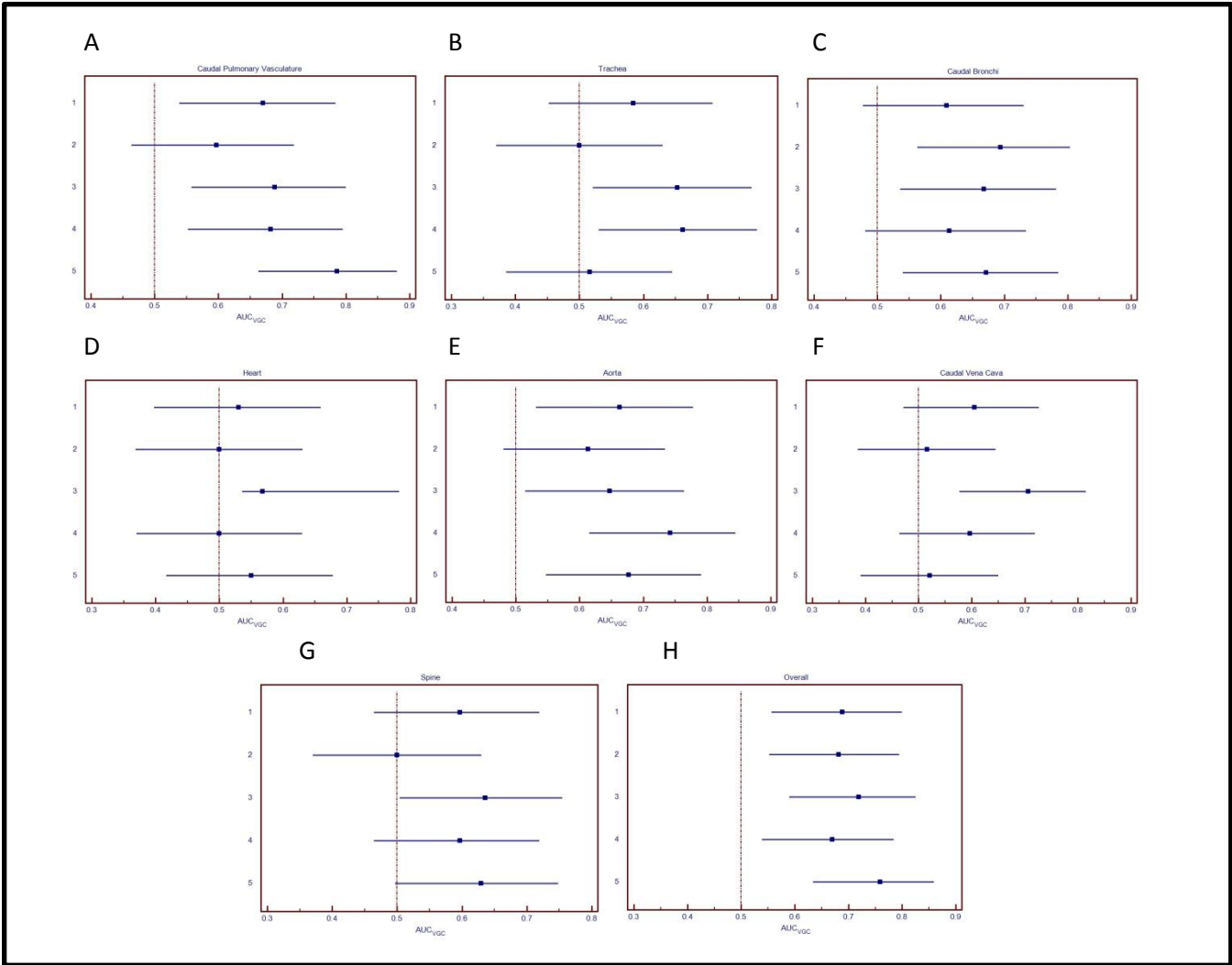


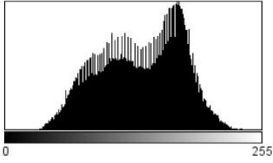
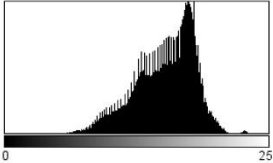
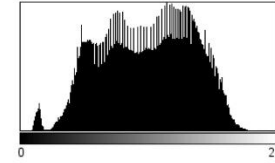
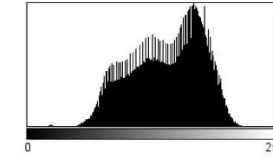
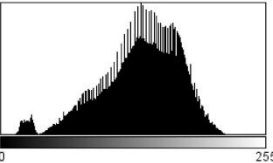
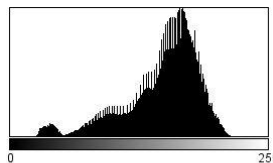
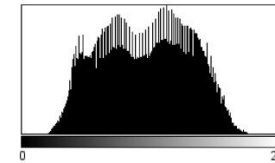
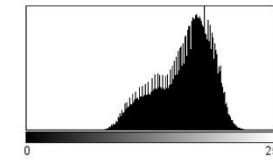
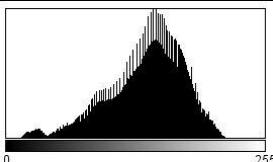
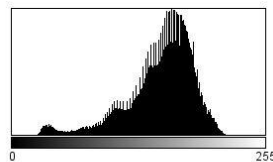
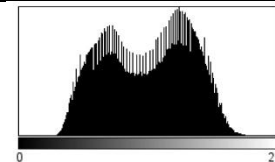
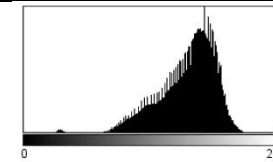
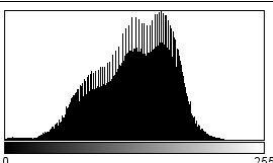
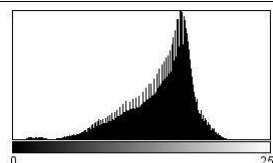
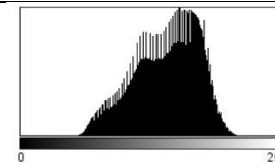
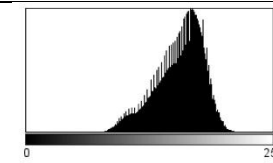
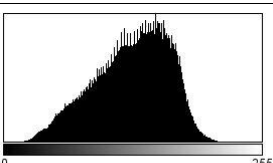
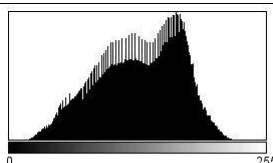
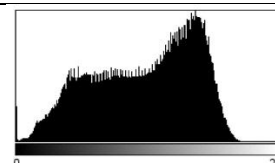
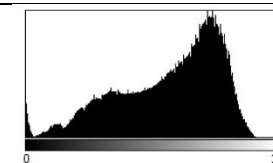
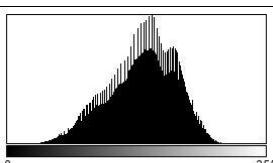
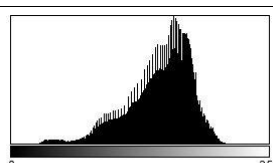
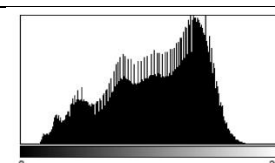
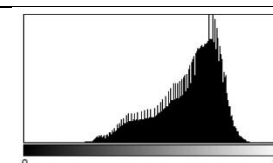
Figure 6. Forest plots of AUCVGC and 95% confidence interval for all observers for the (A) caudal vasculature, (B) trachea, (C) caudal bronchi, (D) heart, (E) Aorta, (F) caudal vena cava, (G) spine, and (H) overall image quality for the lateral images. A vertical line is present at an AUC of 0.5 for reference.

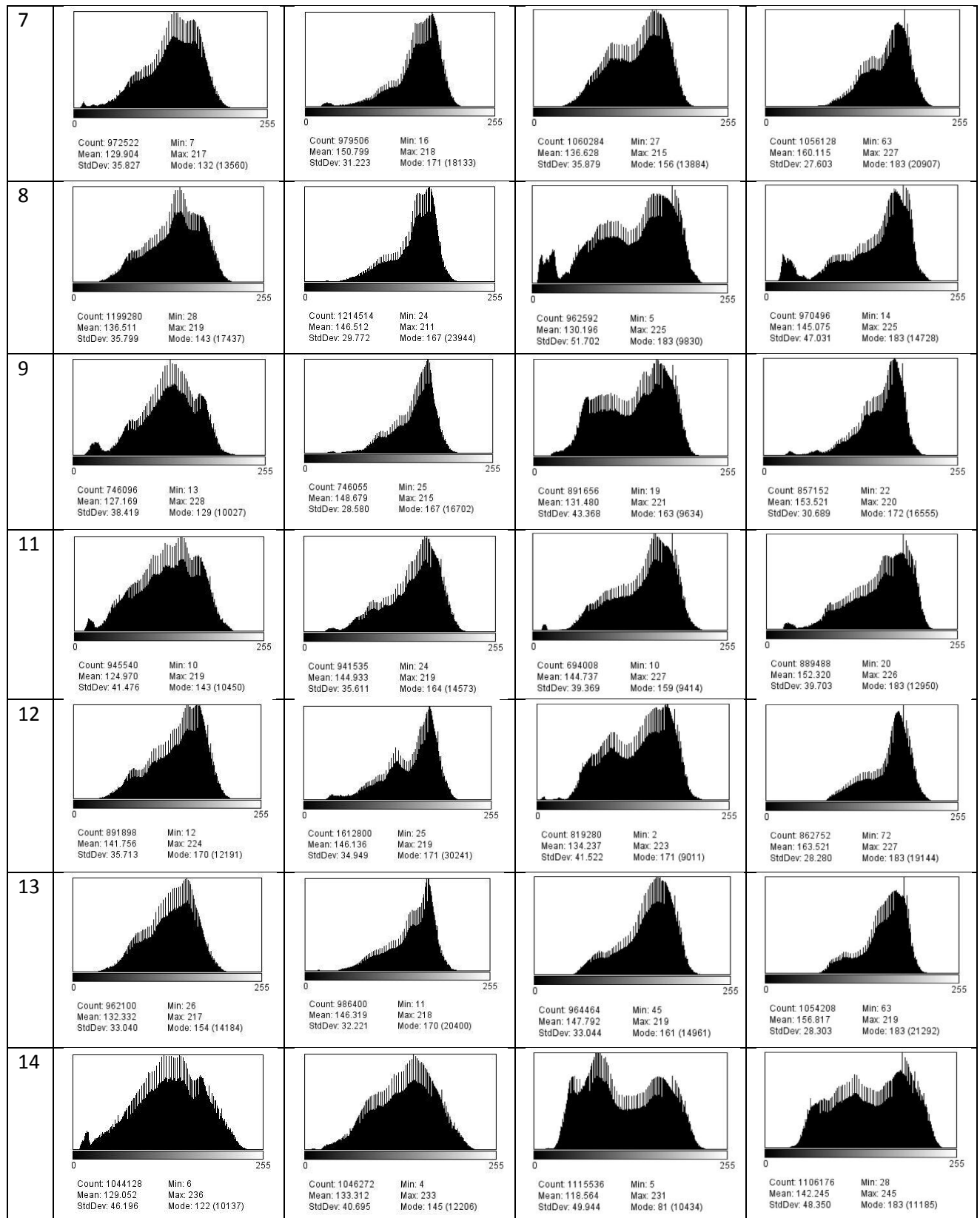
As stated, all observers perceived significantly higher overall image quality for the ventrodorsal images with the collimated approach compared to the whole-body. For observer 1, there was significantly higher quality of the caudal pulmonary vasculature and the aorta on the ventrodorsal images with the collimated approach. For observer 2, there was significantly higher quality for the caudal bronchi on the ventrodorsal images with the collimated approach. For observer 3, the collimated approach for the caudal pulmonary vasculature, trachea, caudal bronchi, caudal vena cava, aorta, and spine had significantly higher quality for the ventrodorsal images. For observer 4, the trachea, heart, and

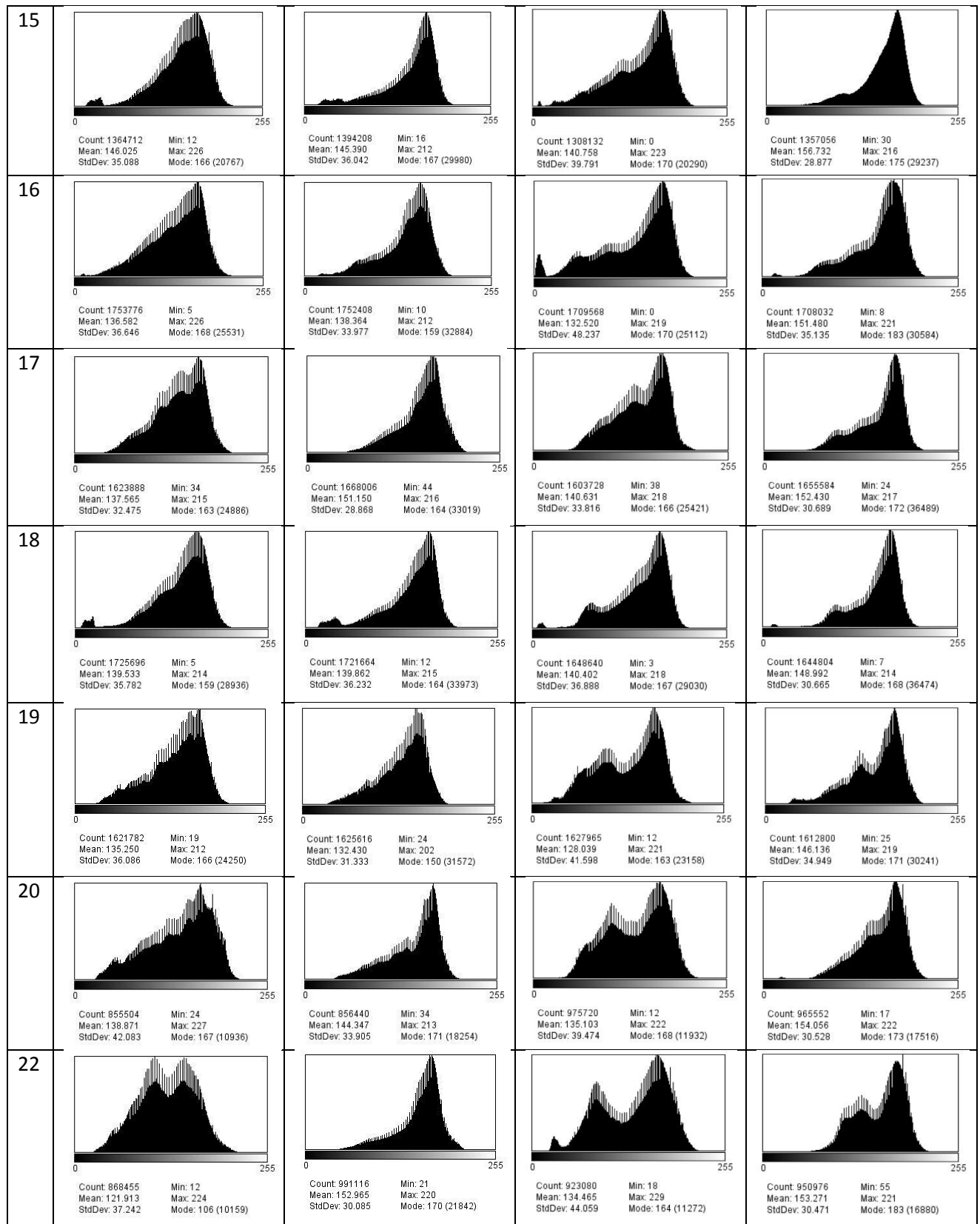
ribs for the lateral images and for the caudal pulmonary vasculature, trachea, and aorta for the ventrodorsal images had higher quality in the collimated approach. Observer 4 also found significantly higher overall quality for the collimated approach for the lateral images. For observer 5, there was significantly higher quality for the caudal pulmonary vasculature, the caudal bronchi, and the aorta on the ventrodorsal images with the collimated approach (**Table 11, Fig.4-5**).

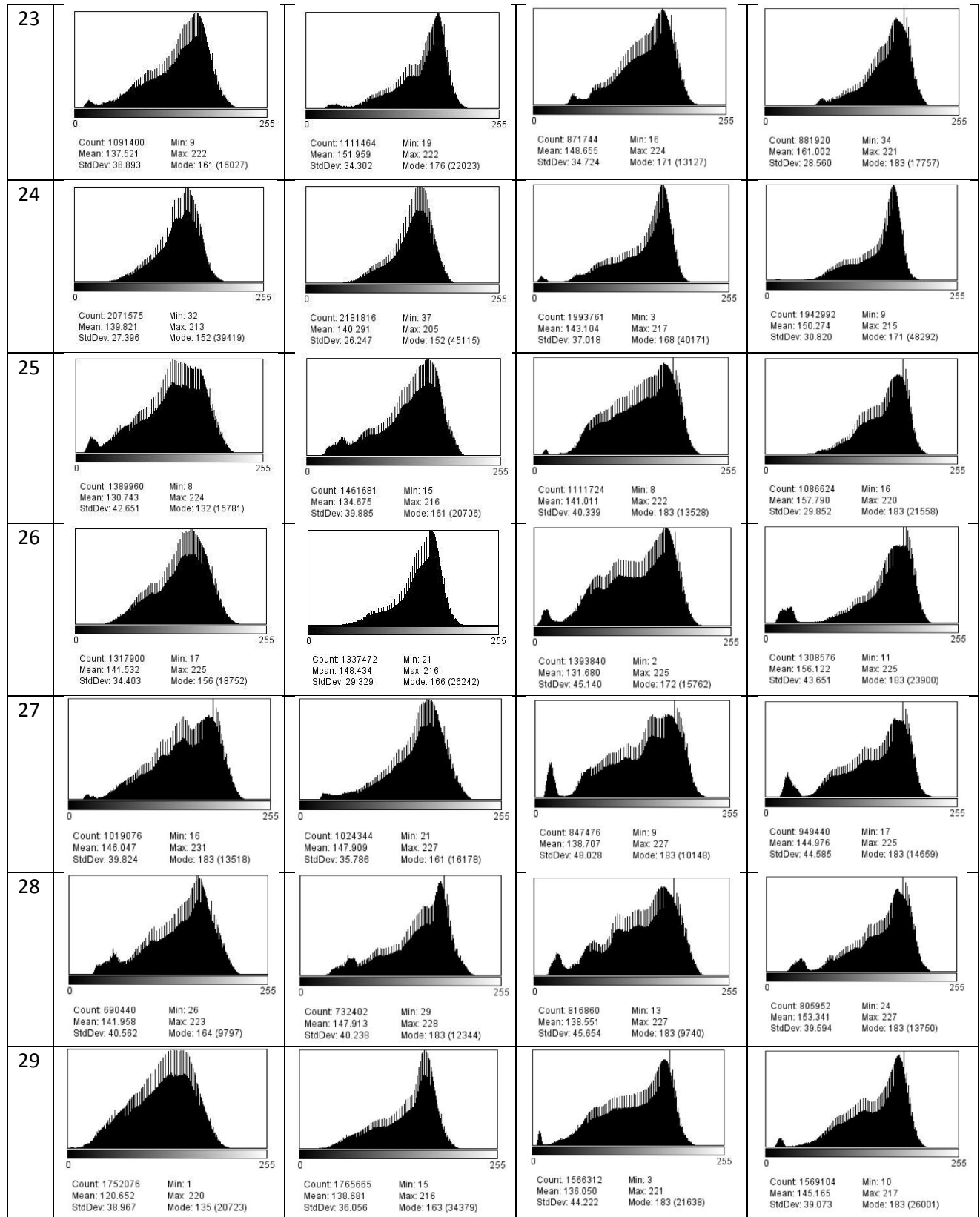
Histograms of the grayscales for all of the cropped images were obtained, and the collimated and whole-body projections for each patient were compared (**Table 12**). Almost all of the histograms for the images obtained with the collimated approach displayed a wider distribution of pixel values, as evidenced by the shape of the distribution and the larger standard deviation. In only six image pairs (four in the lateral, two in the ventrodorsal) was the standard deviation of the collimated images smaller than the standard deviation of the whole-body images. The histograms for the images obtained with the whole-body approach had narrower, taller distributions, and their pixels values were shifted to the higher (whiter) numbers. In most pairs the whole-body images had higher mean pixel values than the matching collimated images. In only three pairs, all in the lateral images, was the mean pixel value of the collimated image higher than the mean pixel value of the whole-body. In all other cases the whole-body images had a higher mean pixel value. In all cases the modes of the whole-body images were greater than or equal to the modes of the matching collimated image.

Table 12. Grayscale histograms for all of the cropped images.

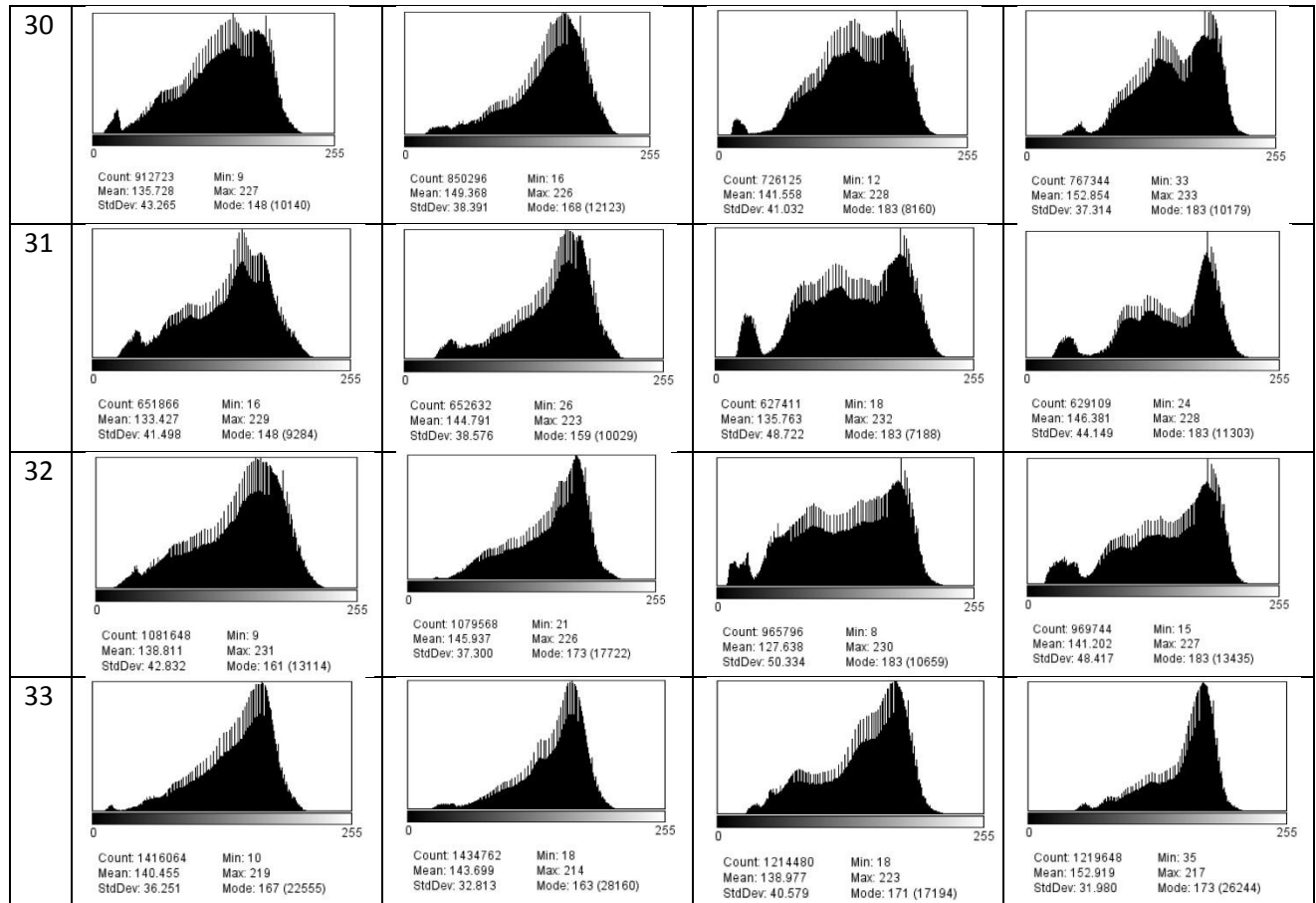
	Lateral		Ventrodorsal	
#	Collimated	Whole-Body	Collimated	Whole-Body
1	 <p>Count: 417032    Min: 29 Mean: 134.825    Max: 240 StdDev: 41.233    Mode: 171 (4827)</p>	 <p>Count: 429408    Min: 53 Mean: 154.725    Max: 238 StdDev: 28.922    Mode: 177 (7865)</p>	 <p>Count: 545076    Min: 11 Mean: 124.851    Max: 230 StdDev: 45.405    Mode: 145 (4840)</p>	 <p>Count: 559980    Min: 20 Mean: 143.581    Max: 227 StdDev: 37.094    Mode: 172 (7046)</p>
2	 <p>Count: 552525    Min: 11 Mean: 133.868    Max: 224 StdDev: 38.568    Mode: 135 (7313)</p>	 <p>Count: 569772    Min: 23 Mean: 150.432    Max: 225 StdDev: 37.032    Mode: 168 (9527)</p>	 <p>Count: 592960    Min: 24 Mean: 121.625    Max: 233 StdDev: 44.202    Mode: 143 (5414)</p>	 <p>Count: 582496    Min: 72 Mean: 161.911    Max: 229 StdDev: 28.699    Mode: 183 (10376)</p>
3	 <p>Count: 579072    Min: 13 Mean: 137.894    Max: 220 StdDev: 37.584    Mode: 148 (8332)</p>	 <p>Count: 580736    Min: 24 Mean: 149.532    Max: 225 StdDev: 34.029    Mode: 161 (9845)</p>	 <p>Count: 598420    Min: 31 Mean: 126.444    Max: 230 StdDev: 42.911    Mode: 158 (6014)</p>	 <p>Count: 591552    Min: 30 Mean: 165.482    Max: 227 StdDev: 28.684    Mode: 183 (12034)</p>
4	 <p>Count: 848928    Min: 0 Mean: 126.436    Max: 227 StdDev: 37.191    Mode: 154 (10576)</p>	 <p>Count: 994008    Min: 11 Mean: 145.610    Max: 219 StdDev: 32.958    Mode: 167 (21504)</p>	 <p>Count: 1039680    Min: 50 Mean: 145.078    Max: 222 StdDev: 32.097    Mode: 158 (13813)</p>	 <p>Count: 1036032    Min: 65 Mean: 158.310    Max: 221 StdDev: 24.850    Mode: 170 (19863)</p>
5	 <p>Count: 2097144    Min: 14 Mean: 125.858    Max: 223 StdDev: 36.990    Mode: 150 (24186)</p>	 <p>Count: 2097144    Min: 15 Mean: 128.958    Max: 231 StdDev: 41.530    Mode: 166 (22565)</p>	 <p>Count: 2378052    Min: 0 Mean: 123.738    Max: 229 StdDev: 50.053    Mode: 174 (23007)</p>	 <p>Count: 2205216    Min: 0 Mean: 143.178    Max: 239 StdDev: 50.615    Mode: 182 (24920)</p>
6	 <p>Count: 863418    Min: 25 Mean: 132.845    Max: 216 StdDev: 33.322    Mode: 143 (12975)</p>	 <p>Count: 883350    Min: 24 Mean: 146.582    Max: 219 StdDev: 32.011    Mode: 161 (15603)</p>	 <p>Count: 831872    Min: 17 Mean: 131.736    Max: 227 StdDev: 45.837    Mode: 171 (9051)</p>	 <p>Count: 831872    Min: 50 Mean: 162.036    Max: 227 StdDev: 32.019    Mode: 183 (16364)</p>











### **Scatter Radiation**

The mean scatter radiation for the collimated lateral projections was 0.3849  $\mu\text{Gy}$  (44.26  $\mu\text{R}$ ) (range 0.1122-1.277 $\mu\text{Gy}$ ). The mean scatter radiation for the whole-body lateral projections was 0.8722  $\mu\text{Gy}$  (100.256  $\mu\text{R}$ ) (range 0.4113-1.948  $\mu\text{Gy}$ ). The mean scatter radiation for the collimated ventrodorsal projections was 0.4035  $\mu\text{Gy}$  (46.4  $\mu\text{R}$ ) (range 0.1435-0.8435  $\mu\text{Gy}$ ). The mean scatter radiation for the whole-body ventrodorsal projections was 1.02  $\mu\text{Gy}$  (117.34  $\mu\text{R}$ ) (range 0.3557-1.835  $\mu\text{Gy}$ ). There was significantly greater scatter radiation produced in the whole-body projections compared to the collimated projections.

Patient weight was highly correlated with the scatter radiation produced in all four projections types. Lateral to lateral width was moderately correlated with scatter detected on collimated ( $R=0.4473$ ,  $p = 0.0324$ ) and whole-body ( $R=0.4757$ ,  $p=0.0252$ ) lateral projections. Ventral to dorsal thickness was moderately to highly correlated with scatter detected on all four projections.

## VI. Discussion

In these results, there was a common trend towards higher image quality and better portrayal of anatomic structures in the collimated images compared to the whole body images. This trend was not always statistically significant, but was strongly consistent between different evaluated structures and different observers. This fits with the traditional view that collimated projections produce higher quality images than whole-body projections. However, because the majority of ratings did not reach statistical significance, the results of this study do not provide clear evidence that digital radiographs produced with a collimated approach are higher quality than those produced with a whole-body approach in their portrayal of normal thoracic anatomy. It is possible that a larger number of cases or pooling grades from multiple observers would provide a large enough sample size to reach statistical significance. However, this would also suggest a relatively modest difference between the two approaches.

Evaluation of the image histograms provided some supporting evidence as to why this trend towards better ratings for the collimated approach exists. The wider, more left shifted histograms of the collimated images indicate more use of blacker pixels. For the thorax, this is especially important, as the portrayal of anatomic detail is enhanced by the contrast provided by the air-filled lungs. Many of the collimated image histograms also showed a wider distribution of pixel values, and some had a bimodal distribution shape that indicates that pixels are grouped around two different extremes. This kind of distribution would be expected in a higher contrast image. The whole-body histograms have narrower peaks consistent with higher latitude images. This is confirmed by subjective comparison of the two images, with the collimated images having a higher contrast appearance and the whole-body images

having a higher latitude appearance. This higher latitude—and thus lower contrast—appearance may contribute to the trend towards lower ratings. The borders of the anatomic structures evaluated will be less accentuated with lower contrast than they would be on a higher contrast image, which may contribute to the observers rating the portrayal of normal anatomy and the overall image quality slightly lower.

Because the grayscale of the images are assigned in processing by the look-up table, these findings from the histograms may indicate that a major component in any difference between the two imaging approach comes from the digital processing of the images. With the whole-body projections the processing computer must account for a much larger range of anatomy and more highly exposed portions of the detector around the patient. This affects how the grayscale is assigned in the final image, which raises the possibility that altering the processing algorithm and look-up table for whole-body projections can make them even more similar to collimated projections in image quality.

The greater amount of scatter radiation produced in the whole-body projections may also influence this appearance. Scatter radiation is well-known to decrease image contrast, which is reflected in the histograms of the whole-body images. However, scatter radiation would also be expected to shift the mean pixel value towards the blacker pixels rather than towards the white pixels. Also, studies have found that modern multiscale processing like the type used in this study mitigates the effects of scatter to a similar degree as a physical grid.<sup>9</sup>

The strongest results were in the ventrodorsal projections, with all observers giving the collimated approach an overall significantly higher image quality rating than the whole-body approach. The difference in overall quality was not significant for most of the observers for the lateral image pairs. In addition, more individual anatomic structures were rated significantly higher in the collimated approach than the whole-body approach for the ventrodorsal image sets compared to the lateral sets. The cause for this may be found in comparing the histograms of the images. The histograms were more

similar overall in the lateral pairs than the ventrodorsal pairs, and there were more cases in the lateral pairs in which the mean pixel value of the collimated images was higher than that of the whole-body images as well as more cases in which the standard deviation of the collimated images was lower than that of the whole-body images.

The lack of strong correlation in ratings between observers indicates one of the drawbacks of visual grading analysis. In an absolute visual grading analysis study like this one, observers draw on the description of the criteria, initial training, and their own clinical experience to rate the fulfillment of certain criteria on an ordinal scale. It is not unusual for VGA/VGC studies to have low observer correlation in grading due to differences in the baselines each observer chooses for their grades.<sup>60</sup> Some observers will be stricter and others more lenient overall in what images and structures they find adequate or high quality. However, a lack of correlation may support the concern that visual grading analysis studies amount to a beauty contest, rather than offering a valid means of comparison in the performance of different diagnostic imaging approaches.

In this case, all of the observers were drawn from the same hospital and were familiar with the digital imaging equipment used in this study. The standard imaging technique at this hospital involves more collimation than in the whole-body approach of this study, but is not as tightly collimated as in the collimated approach. Therefore, the observers were unlikely to be just stating their preference for the images with which they were most familiar from normal clinical practice. In addition, the disparity between observers suggests that they were evaluating the images based on their own individual standards. Because the observers were familiar with the same imaging approach in clinical practice, if they were merely expressing a preference for that approach alone the overall correlation would have been higher.

These results are still meaningful despite the lack of correlation on individual ratings. Although observers differed in how they applied the different grade levels, they all followed the same general

trend in comparing the two imaging approaches. This indicates that, regardless of how strict an observer was in applying the highest grades, they were overall similar in giving, on average, higher grades to the collimated images than the whole-body. More rigorous training or the use of a comparative relative VGA approach may have helped improve correlation in this study.

This study may have also been approached with a relative VGA system rather than the absolute VGA system used. In this case, rather than compare the individual images to a single ideal reference, the matched collimated and whole-body images from each subject could have been presented to the blinded observer at the same time. The observer would have been called upon to state a preference for one image or the other. This would have allowed the most direct comparison of the imaging approaches. However, because the observer would be expressing a preference for one image over another it would not have given a clear indication of the subjective appraisal of individual approaches in isolation. In this study the observers found the vast majority of the images to be of adequate to high quality, regardless of approach. This is valuable information, since it indicates that although there was a trend towards preferring the collimated approach most of the whole-body images were still considered adequate for clinical use. A more strictly comparative study may have shown this preference towards the collimated images without evidence that the whole-body images were also generally adequate to high quality.

Overall, the VGA system provided an easy and convenient way to compare two similar imaging approaches, consistent with the findings from other studies using this technique. Enrolling subjects was simplified, because all normal patients fitting within the study parameters for size and age could be used. There was no need to seek out or wait for patients with a single disease or to modify the images to contain artificial lesions. Each observer was able to complete their task in grading 124 images each within approximately two to three hours, indicating that the study required minimal time from observers compared to more intensive studies such as ROC analysis. This factor likely facilitated

recruitment of observers to contribute to the study as well. While VGA and VGC studies cannot replace ROC studies in fully evaluating the diagnostic performance of an imaging system, they are very helpful in supplying a relatively simple way to compare similar imaging approaches. This provides an initial benchmark for future research. The VGA approach is also well-suited for individual institutions evaluating a possible change in an imaging protocol.

As expected, the whole-body projections produced significantly more scatter radiation. This follows the well-known principle that scatter radiation increases with field size. It is an important component to consider, due to the common presence of personnel within the room during veterinary radiographic examinations. Because of this difference in scatter, the principles of ALARA suggest that whole-body images should be avoided unless necessary regardless of any image quality implications. The fact that the mean scatter radiation detected for the whole-body projections was over twice that for the collimated projections also suggests that staff exposure should be similar for doing individual projections of the thorax and abdomen compared to single whole-body projections. Whole-body projections may provide benefits in terms of efficiency (decreased time for a radiographic examination of the thorax and abdomen) and stress to the patient due to restraint, but would not provide benefits in regards to staff exposure.

Even with the differences in subjective quality between the imaging approaches identified in this study, overall quality for all images was high. Out of over 600 observer ratings for individual images, only 7.58% were considered to be below adequate. Whatever quality difference there is between collimated and whole-body approaches, both approaches overwhelmingly produced images of adequate to high quality for clinical use when using a modern digital radiography system. Although this study provides some evidence that the whole-body approach produces lower quality images even with the advantages of digital radiography, the whole-body images remained of at least adequate quality.

The next question, therefore, is whether the relatively modest difference in quality identified in this study causes a significant effect on diagnostic performance in clinical cases. Because radiography is about identifying changes in the normal anatomy, it is reasonable that the imaging approach that produces the best portrayal of normal anatomy will yield the most accurate clinical performance. However, even a more significant and robust quality difference than identified in this study does not necessarily indicate a significant change in diagnostic performance. Based on the factors identified in evaluating the histograms of these images, there may be some concern that the whole-body projections will suffer in their diagnostic performance for pulmonary abnormalities. Most pulmonary abnormalities manifest as regions of increased opacity within the air-filled lungs. The whole-body images had overall higher latitude with the mean pixel values shifted towards the whiter end of the spectrum. The higher pixel values throughout the lung field may obscure identification of subtle increases in opacity within the lungs. The logical next step in evaluation of these imaging approaches is an ROC study comparing their diagnostic performance in identification of subtle pulmonary abnormalities, such as small pulmonary nodules.

One key caveat from this study is that these results cannot necessarily be generalized to other digital radiographic systems or other digital processing protocols. This is especially true since the processing and applied look-up table appear to be an important difference in the final images produced by the two imaging approaches. Other digital processing protocols may do a better or worse job in matching the grayscale appearance of the two images, which could significantly impact the subjective difference in image quality.

Given these findings, clinical bias should remain towards obtaining appropriate collimated projections—even with modern digital radiography—pending the results of further research. This approach is most likely to produce the highest quality images and satisfies the obligation to keep radiation exposure to personnel as low as reasonably achievable. Future research comparing the



diagnostic performance of these two imaging approaches on a common clinical question is needed to fully guide selection of appropriate digital radiography techniques for small animal patients.

## V. References

1. Bushberg JT, Seibert JA, Leidholdt EM et al. *The Essential Physics of Medical Imaging*. 3<sup>rd</sup> Ed. Philadelphia: Lippincott Williams & Wilkins, 2012.
2. Curry TS, Dowdey JE, Murry RC. *Christensen's Physics of Diagnostic Radiology*. 4<sup>th</sup> ed. Philadelphia: Lea & Febiger, 1990.
3. Shueler BA. Clinical applications of basic x-ray physics principles. *Radiographics*. 1998;18(3):731-44.
4. Mattoon JS. Digital radiography. *Vet Comp Orthop Traumatol*. 2006;19:123-32.
5. Morgan JP, Silverman S. *Techniques of Veterinary Radiography*. 3<sup>rd</sup> ed. Davis: Veterinary Radiology Associates, 1982.
6. Mettler FA, Sinclair W. The 1986 and 1988 UNSCEAR reports: findings and implications. *Health Phys* 1990;158:241-150.
7. Widmer WR, Shaw SM, Thrall, DE. Effects of low level exposure to ionizing radiation: current concepts and concerns for veterinary workers. *Vet Radiol Ultrasoun*. 1996;37(3):227-239.
8. Spahn M. Flat detectors and their clinical applications. *Eur Radiol* 2005;15: 1934–1947.
9. Lo WY, Zwingenberger AL, Robertson ID. Multiscale image processing and anti-scatter grids in digital radiography. *Vet Radiol Ultrasoun*. 2009;50(6):569-76.
10. Uffman M, Schaefer-Prokob C. Digital radiography: The balance between image quality and required radiation dose. *Eur Radiol*. 2009;72:202-208.
11. Lo WY, Puchalski SM. Digital imaging processing. *Vet Radiol Ultrasoun*. 2008;49(S1):S42-S47.
12. SamuelS, Kundel HL, Nodine CF, Toto LC. Mechanism of satisfaction of search: eye position recordings in the reading of chest radiographs. *Radiology*. 1995; 194:895-902.
13. Berbaum KS, Franken JEA, Dorfman DD, et al. Role of faulty visual search in the satisfaction of search effect in chest radiography. *Acad Radiol* 1998; 5:9-19.
14. Berbaum et al. Gaze dwell times on acute trauma injuries missed because of satisfaction of search. *Acad Radiol*. 2001 Apr;8(4):304-14.
15. Wright M. With digital radiography it is ok to take veterinary whole body radiographs. Available at: <http://animalinsides.com/learn/digital-imaging/178-with-digital-radiography-it-is-ok-to-take-veterinary-whole-body-radiographs-.html> . Accessed 7/17/11).
16. Busch HP, Lehmann KJ, Drescher P, et al. New chest imaging techniques: a comparison of five analogue and digital methods. *Eur Radiol* 1992;2:335–341.
17. Ishigaki T, Endo T, Ikeda M, et al. Subtle pulmonary disease: detection with computed radiography versus conventional chest radiography. *Radiology* 1996;201:51–60.

18. van Heesewijk HP, van der Graaf Y, de Valois JC, et al. Chest imaging with a selenium detector versus conventional film radiography: a CT controlled study. *Radiology* 1996;200:687–690.
19. Kotter E, Einert A, Merz C, et al. Comparison between a screen-film system and a selenium radiography system. An ROC study using simulated thoracic lesions. *Invest Radiol.* 1999;34:296–302.
20. Schaefer-Prokop CM, Prokop M, Schmidt A, et al. Selenium radiography versus storage phosphor and conventional radiography in the detection of simulated chest lesions. *Radiology.* 1996;201:45–50.
21. Strotzer M, Gmeinwieser J, Voelk M, et al. Detection of simulated chest lesions with normal and reduced radiation dose: comparison of conventional screen-film radiography and a flat-panel X-ray detector based on amorphous silicon. *Invest Radiol.* 1998;33:98–103.
22. Strotzer M, Gmeinwieser J, Volk M, et al. Clinical application of a flat-panel X-ray detector based on amorphous silicon technology: image quality and potential for radiation dose reduction in skeletal radiography. *Am J Roentgenol* 1998;171:23–27.
23. Strotzer M, Gmeinwieser JK, Spahn M et al. Amorphous silicon, flat-panel, X-ray detector versus screen-film radiography: effect of dose reduction on the detectability of cortical bone defects and fractures. *Invest Radiol.* 1998;33:33-8.
24. Strotzer M, Voelk M, Wild T et al. Stimulated bone erosions in a hand phantom: detection with conventional screen-film technology versus cesium iodide-amorphous silicon flat-panel detector. *Radiology.* 2000;215:512-5.
25. Piraino DW, Davros WJ, Lieber M, et al. Selenium based digital radiography versus conventional film-screen radiography of the hands and feet: a subjective comparison. *Am J Roentgenol.* 1999;172:177–184.
26. Woodard PK, Slone RM, Sagel SS. Detection of CT-proved pulmonary nodules: comparison of selenium-based digital and conventional screen-film chest radiographs. *Radiology* 1998;209:705–709.
27. Schaefer CM, Greene R, Oestmann JW, et al. Digital storage phosphor imaging versus conventional film radiography in CT-documented chest disease. *Radiology.* 1990;174:207–210.
28. Hames S, Freyschmidt J, Neitzel U. Digital radiography with a large-scale electronic flat-panel detector vs screen-film radiography: observer preference in clinical skeletal diagnosis. *Eur Radiol.* 2001;11:1753-1759.
29. Kroft LJ, Veldkamp WJ, Mertens BJ, et al. Comparison of eight different digital chest radiography systems: variation in detection of simulated chest disease. *Amer J Roentgenol* 2005;185(2):339–46.
30. Veldkamp WJ, Kroft LJ, Geleijns J. Dose and perceived image quality in chest radiography. *Eur Radiol.* 2009;72:209–217.
31. Marolf A, Blaik M, Ackerman N, et al. Comparison of computed radiography and conventional radiography in detection of small volume pneumoperitoneum. *Vet Radiol Ultrasoun.* 2008;49(3):227-32.
32. Essmann S, Sherman A. Comparison of digitized and conventional radiographic images for assessment of hip joint conformation in dogs. *Am J Vet Res.* 2006;67:1546–51.

33. Lister SA, Roush JK, Renber WC. Digital measurement of radiographic tibial plateau angle. A comparison to measurement on printed digital images. *Vet Comp Orthop Traumatol*. 2008;21:129-32.
34. Serwa D, Lorinson K, Lorinson D, et al. Comparison of conventional and digital measurements of tibial plateau angle in dogs. *J Am Vet Med Assoc*. 2009;234:622-4.
35. Meyer-Lindenberg A, Ebermaier C, Wolvekamp P, et al. [Comparative evaluation of six different body regions of the dog using analog and digital radiography]. *Berl Munch Tierarztl Wochenschr*. 2008;121(5-6):216-27. (in German).
36. Ludewig E, Hirsch W, Bosch B, et al. [Assessment of clinical image quality in feline chest radiography with a needle image plate (NIP) storage phosphor system—an approach to the evaluation of image quality in neonatal radiography]. *Rofo* 2010;182:122–132. (in German).
37. Masumitsu H, Shibata E. Application of computed radiography system for horse: decrease of X-ray exposure and improvement of X-ray image quality. *Bull Equine Res Inst*. 1990;27:7–14.
38. Bindeus T, Vrba S, Gabler C, et al. Comparison of computed radiography and conventional film-screen radiography of the equine stifle. *Vet Radiol Ultrasoun*. 2002;43(5):455-60.
39. Moorman VJ, Marshall JF, Devine DV, et al. Comparison of flat-panel digital to conventional film-screen radiography in detection of experimentally created lesions of the equine third metacarpal bone. *Vet Radiol Ultrasoun*. 2009;50(6):577-83.
40. Bochmann M, Ludewig E, Krautwald-Junghanns ME, et al. Comparison of the image quality of a high-resolution screen-film system and a digital flat panel detector system in avian radiography. *Vet Radiol Ultrasoun*. 2011;52(3):256-61.
41. Pees M, Bochmann M, Krautwald-Junghanns ME, et al. [Comparative radiography of the respiratory tract of snakes using conventional high-resolution film-screen-system and digital detector system]. *Berl Munch Tierarztl Wochenschr*. 2010;123(5-6):177-85. (in German).
42. Ludwig K, Schulke C, Diedrich S, et al. Detection of subtle undisplaced rib fractures in a porcine model: radiation dose requirement – digital flat-panel versus screen-film and storage-phosphor systems. *Radiology*. 2003;227:163–168).
43. Don S, Hildebolt CF, Sharp TL, et al. Computed radiography versus screen-film radiography: detection of pulmonary edema in a rabbit model that simulates neonatal pulmonary infiltrates. *Radiology* 1999;213:455–460.
44. Ludwig K, Ahlers K, Wormanns D, et al. Lumbar spine radiography: digital flat-panel detector versus screen-film and storage-phosphor systems in monkeys as a pediatric model. *Radiology*. 2003;229:140–144.
45. Zetterberg LG, Espeland A. Lumbar spine radiography—poor collimation practices after implementation of digital technology. *Brit J Radiol*. 2011;84:566-569
46. Bath M. Evaluating imaging systems: practical applications. *Radiat Prot Dosim*. 2010;139(1-3):29-36.
47. van Erkel AR, Pattynama PM. Receiver operating characteristic (ROC) analysis: basic principles and applications in radiology. *Eur Radiol*. 1998;27:88–94.
48. Ludewig E, Richter A, Frame M. Diagnostic Imaging—evaluating image quality using visual grading characteristics (VGC) analysis. *Vet Res Commun*. 2010;34:473–479.

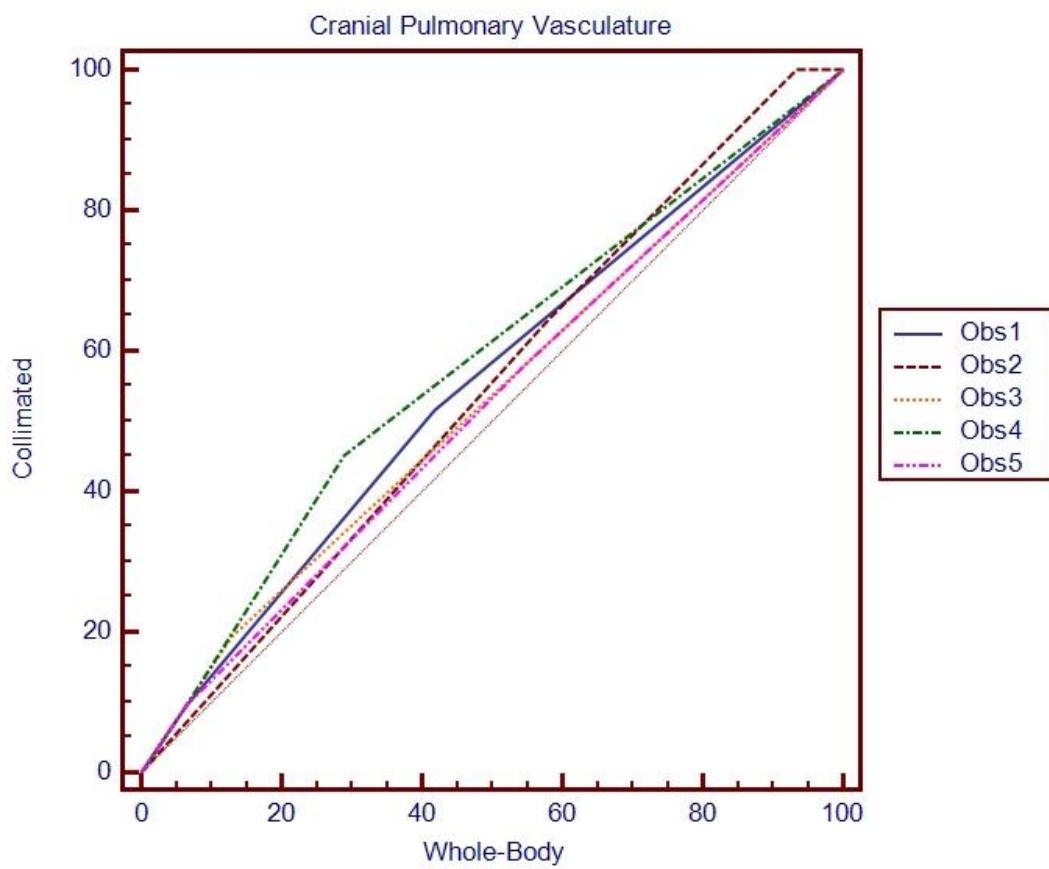
49. Gur D, Rockette HE, Armfield DR, et al. Prevalence effect in a laboratory environment. *Radiology*. 2003;228:10-4.)
50. Gur D, Bandos AI, Fuhman CR, et al. The prevalence effect in a laboratory environment: changing the confidence ratings. *Acad Radiol*. 2007;14:49–53.
51. Bath M, Mansson LG. Visual grading characteristics (VGC) analysis: a non-parametric rank-invariant statistical method for image quality evaluation. *Brit J Radiol*. 2007;80:169-76.
52. Sund P, Herrmann C, Tingberg A, et al. Comparison of two methods for evaluating image quality of chest radiographs. *Proc. SPIE*. 2000;3981:251–257
53. Tingberg A, Herrmann C, Lanhede B, et al. Comparison of two methods for evaluation of the image quality of lumbar spine radiographs. *Radiat Prot Dosim* 2000;90:165–168
54. Sandborg M, McVey G, Dance DR et al. Comparison of model predictions of image quality with results of clinical trials in chest and lumbar spine screen-film imaging. *Radiat Prot Dosim* 2000;90:173–76.
55. Sandborg M, et al. Demonstration of correlations between clinical and physical image quality measures in chest and lumbar spine screen-film radiography. *Brit J Radiol*. 2001;74:520–28.
56. Sandborg M, Tingberg A, Ullman G, Dance DR, et al. Comparison of clinical and physical measures of image quality in chest and pelvis computed radiography at different tube voltages. *Med Phys*. 2006;33:4169–4175.
57. Veldkamp WJ et al. A technique for stimulating the effect of dose reduction on image quality in digital chest radiography. *J Digit Imaging*. 2009;22(2):114-25.
58. Zanca F. et al. Comparison of visual grading and free-response ROC analyses for assessment of image-processing algorithms in digital mammography. *Brit J Radiol*. 2012;85:e1233-41.
59. Tingberg A, Bath M, Hakansson M, Medin J, Besjakov J, Sandborg M, et al. Evaluation of image quality of lumbar spine images: a comparison between FFE and VGA. *Radiat Prot Dosimetry* 2005;114:53–61.
60. Falt T et al. Seesaw balancing radiation dose and I.V. contrast dose: evaluation of a new abdominal CT protocol for reducing age-specific risk. *Am J Roentgenol*. 2013;200;383-8.
61. Commission of the European Communities. *European guidelines on quality criteria for diagnostic radiographic images*. Report EUR 16260 EN. Luxembourg: Office for official publications of the European Communities, 1996.
62. Commission of the European Communities. *European guidelines on quality criteria for diagnostic radiographic images in paediatrics*. Report EUR 16261 EN. Luxembourg: Office for official publications of the European Communities, 1996.
63. Commission of the European Communities. *European guidelines on quality criteria for computed tomography*. Report EUR 16262 EN. Luxembourg: Office for official publications of the European Communities, 1996.
64. Berry CR, Graham JP, Thrall DE. Interpretation paradigms for the small animal thorax. In: Thrall DE (ed): *Textbook of veterinary diagnostic radiology*. Philadelphia: W. B. Saunders, 2007;462–485.
65. Rudolf H, Taeymans O, Johnson V. Basics of thoracic radiography and radiology. In: Schwarz T, Johnson V (eds): *BSAVA Manual of canine and feline thoracic imaging*. Gloucester: BSAVA, 2008;1–19.

66. Chakraborty DP. Problems with the differential receiver operating characteristic (DROC) method. *Proc SPIE*. 2004;5372:138–43.
67. Vucich J, Goodenough DJ, Lewicki A, Briefel E, Weaver KE. Use of anatomical criteria in screen/film selection for portable chest x-ray procedures. In: Cameron J, editor. *Optimization of chest radiography*. HHS Publication 80-8124. Rockville, MD: FDA, 1980:237–48.
68. Ludewig E, Hirsch W, Bosch B, et al. [Assessment of clinical image quality in feline chest radiography with a needle image plate (NIP) storage phosphor system—an approach to the evaluation of image quality in neonatal radiography]. *Rofo* 2010;182:122–132. (in German).
69. Ludewig E et al. Display Quality of Different Monitors in Feline Digital Radiography. *Vet Radiol Ultrasoun*. 2010;52;1-9.
70. Geijer H et al. Comparison of color LCD and medical-grade monochrome LCD displays in diagnostic radiology. *J Digit Imaging*. 2007;20;114-21.
71. Berner K et al. Dose optimisation of double-contrast barium enema examinations. *Radiat Prot Dosimetry*. 2010;139;388-92.
72. Martin L et al. Paediatric x-ray radiation dose reduction and image quality analysis. *J Radiol Prot*. 2013;33;621-33.
73. Precht H et al. Digital radiography: optimization of image quality and dose using multi-frequency software. *Pediatr Radiol*. 2012;42;1112-8.
74. Zachrisson S et al. Optimisation of tube voltage for conventional urography using a Gd2O2S:Tb flat panel detector. *Radiat Prot Dosimetry*. 2010;139;86-91.
75. Leander P et al. Post-processing image filtration enabling dose reduction in standard abdominal CT. *Radiat Prot Dosimetry*. 2010;139;180-5.
76. Burmeister HP et al. Visual grading characteristics (VGC) analysis of diagnostic image quality for high resolution 3 Tesla MRI volumetry of the olfactory bulb. *Acad Radiol*. 2011;18;634-9.
77. Baltzer PA et al. A systematic comparison of two pulse sequences for edema assessment in MR-mammography. *Eur J Radiol*. 2012;81;1500-3.
78. Ragnehead M et al. Visual grading of 2D and 3D functional MRI compared with image-based descriptive measures. *Eur Radiol*. 2010;20;714-24.
79. Jacobson GA, Van Forowe DE. Survey of x-ray protection practices among Michigan veterinarians. *J Am Vet Med Assoc*, 1964;145:793-7
80. Sullivan RJ, Keene BE, Sachs M et al. A survey of x-radiation exposure in the practice of veterinary medicine. *Public Health Rep*. 1957;72(10):883-887.
81. O'Riordan MC. X-ray hazards in practices. *Vet Rec* 1970;87:640-3.
82. Blair, A. and H.M. Hayes: Mortality Patterns among US Veterinarians. 1947-1977: An Expanded Study. *Int. J. Epidemiol*. 1982;11;391-7
83. Wiggins P, Schenker MB, Green R et al. (1989) Prevalence of hazardous exposures in veterinary practice. *Am J Ind Med* 16:55–66.
84. Fritschi L, Shirangi A, Roberston ID. Trends in exposure of veterinarians to physical and chemical hazards and use of protection practices. *Int Arch Occup Environ Health*. 2008;81:371–378.
85. Wrigley RH, Borak TB. The effect of kVp on the dose equivalent received from scattered radiation by radiography personnel. *Vet Radiol*. 1983;24(4):181-185.

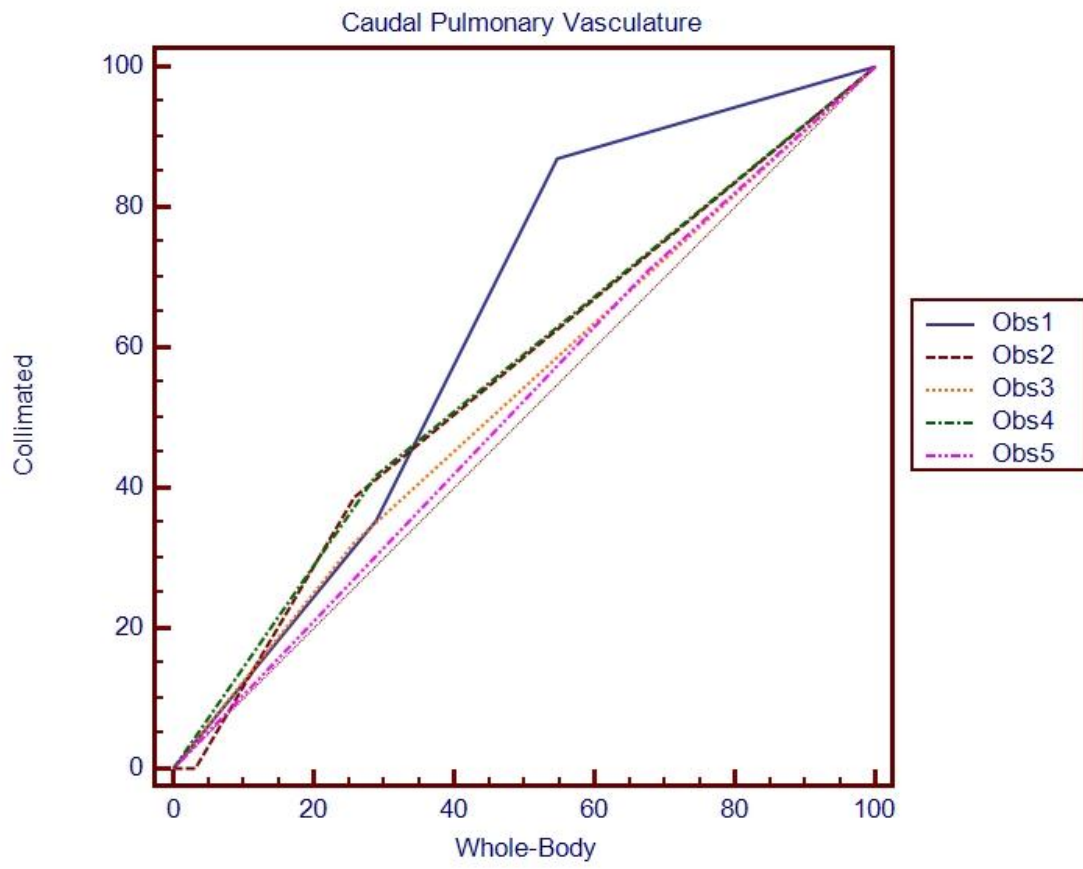
86. Sullivan RJ, Keene BE, Sachs M et al. A survey of x-radiation exposure in the practice of veterinary medicine. *Public Health Rep.* 1957;72(10):883-887.

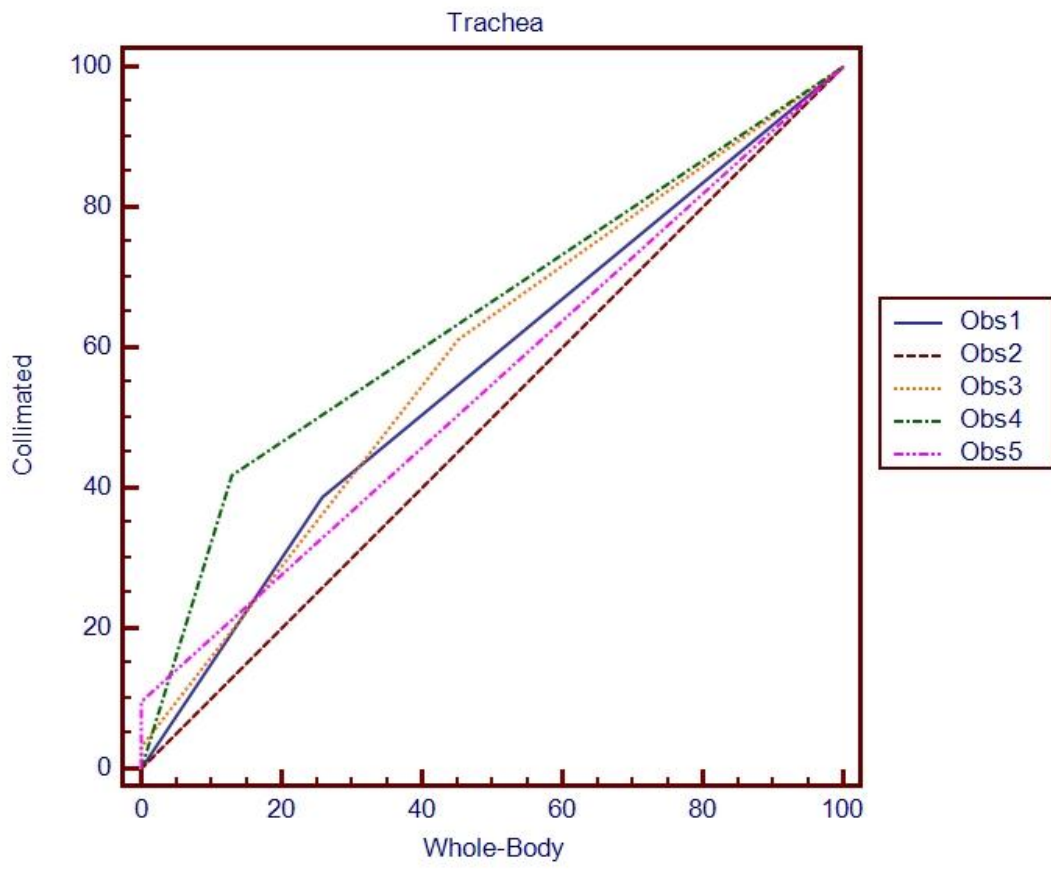
**Appendix A:  
VGC curves for all criteria**

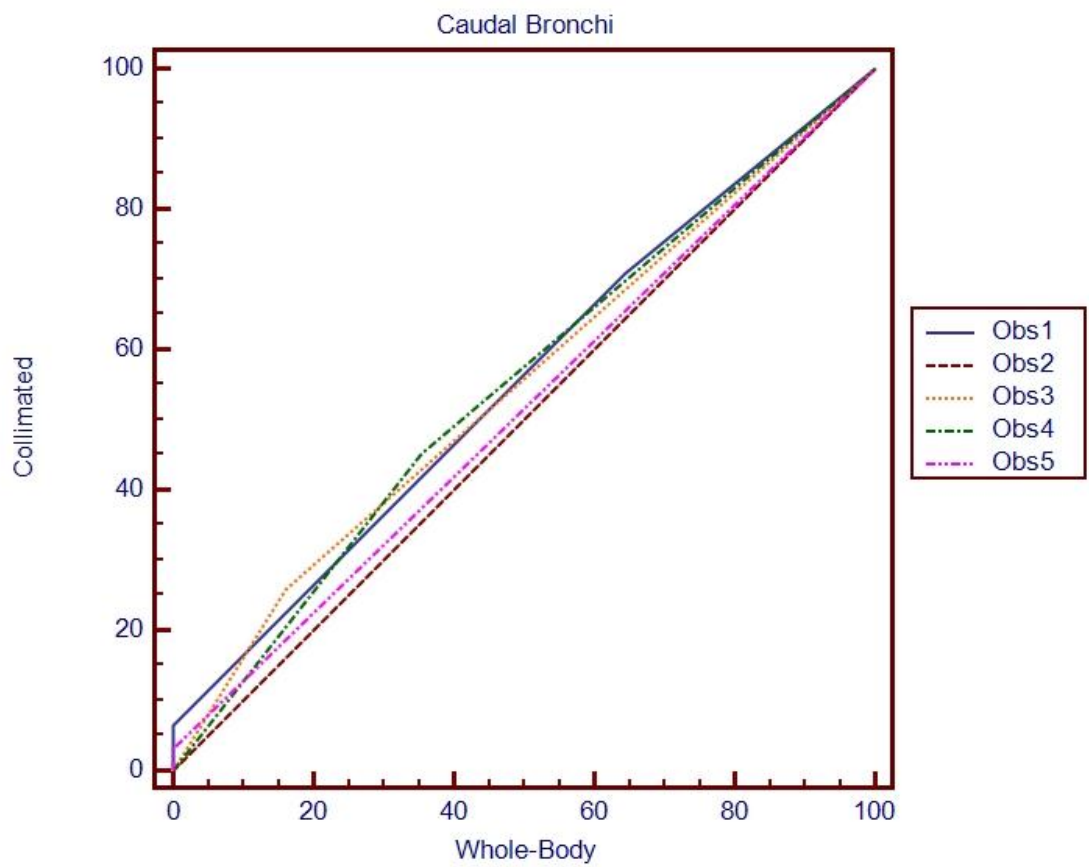
**LATERAL**

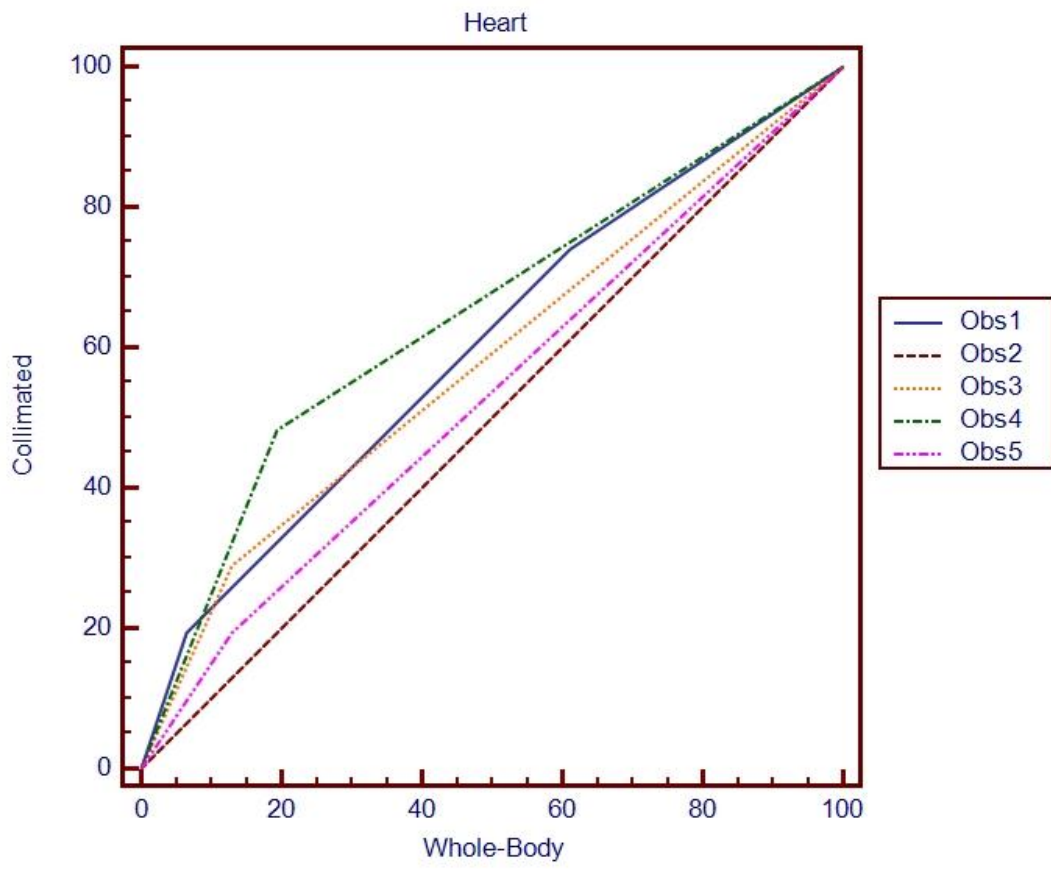


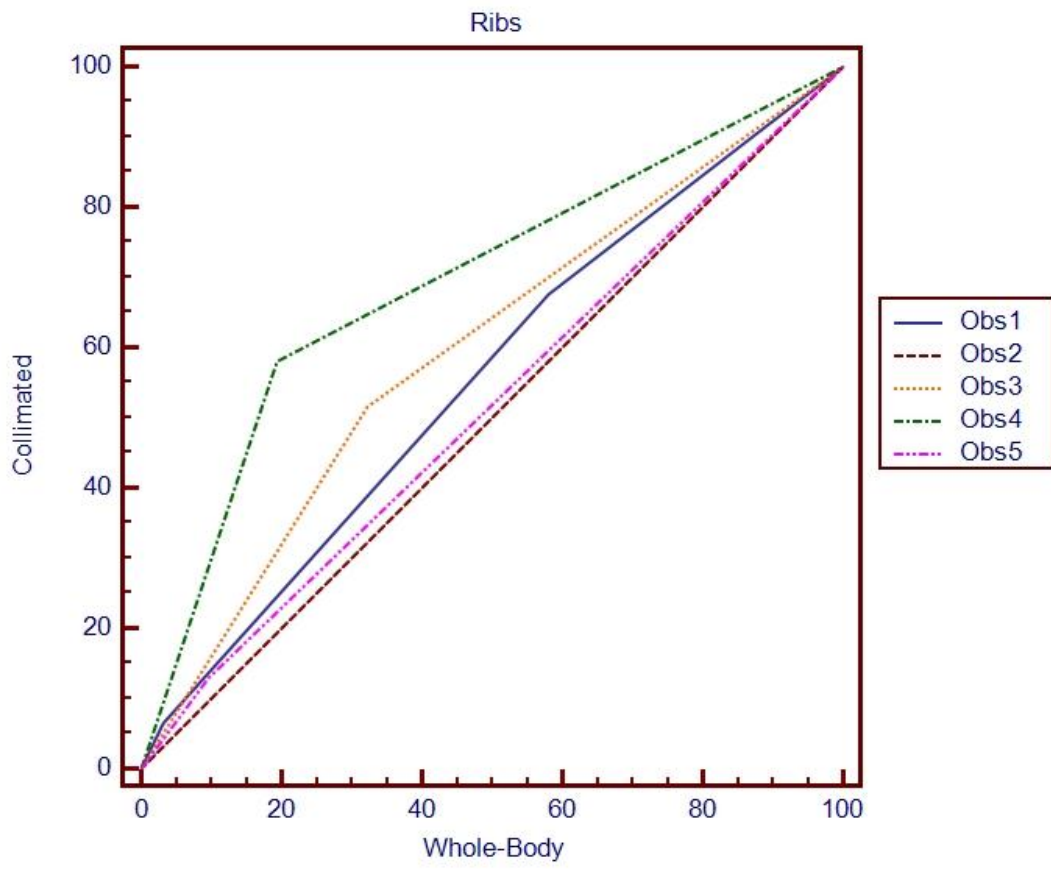


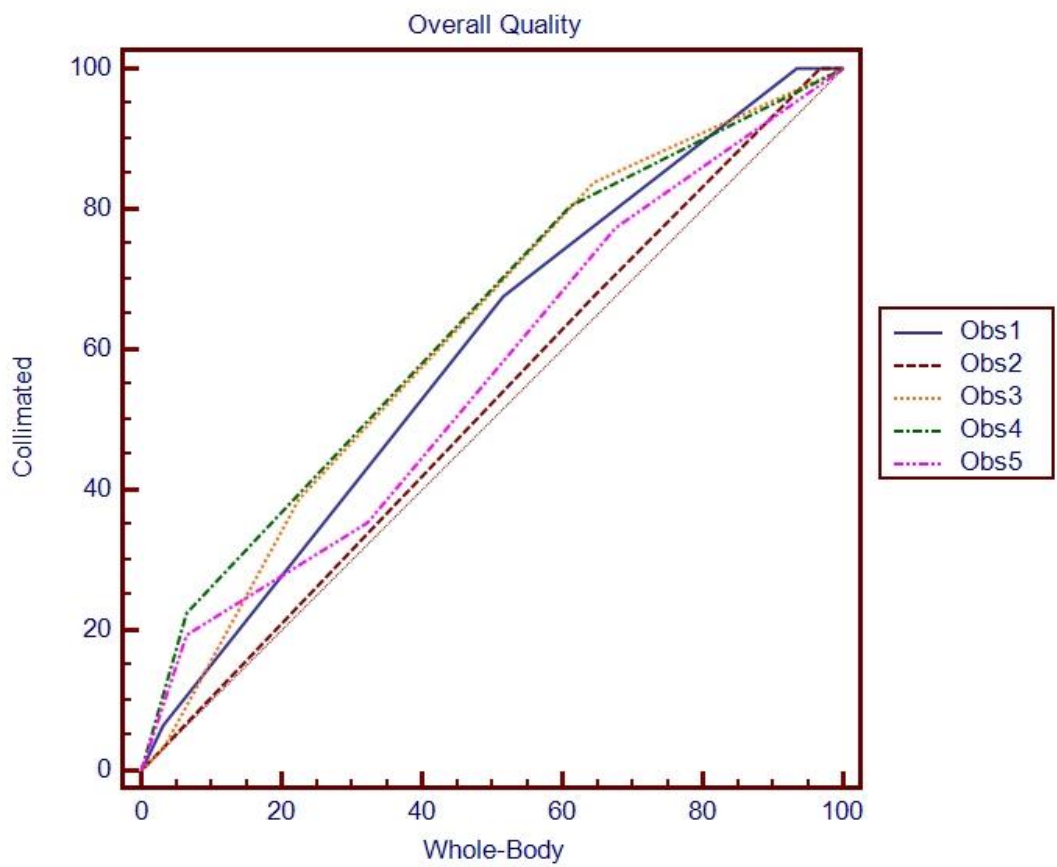












## Ventrodorsal

